https://ntrs.nasa.gov/search.jsp?R=19780004072 2020-03-22T06:43:47+00:00Z

REPORT NO. AFL 77-11-36

Department of Aerospace Engineering
University of Cincinnati

(NASA-CR-155329) SUPERSONIC SEPARATED TURBULENT BOUNDARY - LAYER OVER A WAVY WALL (Cincinnati Univ.) 66 p HC A04/MF A01 CSCL 01A

N78-12015

Unclas
G3/02 53611

SUPERSONIC SEPARATED TURBULENT BOUNDARY-LAYER OVER A WAVY WALL

A. POLAK

AND

M.J. WERLE

This research was supported by NASA Langley Research Center under Grant No. NSG 1208.

Distribution of this report is unlimited.

RECEIVED
DEC 1977
NASA STI FACILITY

November 1977

SUPERSONIC SEPARATED TURBULENT BOUNDARY-LAYER OVER A WAVY WALL*

A. Polak**

and

M.J. Werle**

Department of Aerospace Engineering and Applied Mechanics
University of Cincinnati
Cincinnati, Ohio 45221

November 1977

* This research was supported by NASA Langley Research Center under Grant No. NSG 1208.

** Professor

FORWARD

This research was supported by NASA Langley Grant No. NSG 1208. The NASA Technical Officer for this grant was Mr. James C. Dunavant, NASA Langley Research Center.

The authors wish to gratefully acknowledge the continued interest and technical guidance of Prof. R.T. Davis of the University of Cincinnati.

SUPERSONIC SEPARATED TURBULENT BOUNDARY-LAYER OVER A WAVY WALL

by

A. Polak and M.J. Werle
University of Cincinnati

SUMMARY

This research is concerned with the development of a prediction method for calculating detailed distributions of surface heating rates, pressure and skin friction over a wavy wall in a two-dimensional supersonic flow. Of particular interest is the flow of thick turbulent boundary layers. The surface geometry and the flow conditions considered are such that there exists a strong interaction between the viscous and inviscid flow. First, using the interacting turbulent-boundary layer equations, the problem is formulated in physical coordinates and then a reformulation of the governing equations in terms of Levy-Lees variables is given. Next, a numerical scheme for solving interacting boundary layer equations is adapted. A number of modifications which led to the improvement of the numerical algorithm are discussed. Finally, results are presented for flow over a train of up to six waves at various flow conditions. Limited comparisons with independent experimental and analytical results are also given.

ORIGINAL PAGE IS
OF POOR QUALITY

TABLE OF CONTENTS

	Page
INTRODUCTION	1
GOVERNING EQUATIONS	3
NUMERICAL METHOD OF SOLUTION	14
RESULTS AND DISCUSSION	20
CONCLUSIONS	28
REFERENCES	29
APPENDICES	
A. GRID SIZE EFFECT ON ACCURACY	31
B. INITIAL PROFILES FOR THICK BOUNDARY LAYERS	35

NOMENCLATURE

a	Amplitude.
A	Eddy viscosity damping function.
C_f	Skin friction coefficient, $\tau_w^*/\rho_\infty^* u_\infty^{*2}/2$.
C_p	Constant pressure specific heat.
F	Normalized longitudinal velocity, $F = u/u_e$.
g	Normalized total enthalpy, $g = H/H_e$.
h	Heat transfer coefficient.
H	Nondimensional total enthalpy, $H = H^*/u_\infty^{*2}$.
K_1, K_2	Constants in eddy viscosity models.
ℓ	Viscosity parameter, $\ell = \rho\mu/\rho_e\mu_e$.
$\bar{\ell}$	Mixing length.
L^*	Reference length.
M	Mach number.
p	Nondimensional static pressure, $p = p^*/\rho_\infty^* u_\infty^{*2}$.
Pr	Prandtl number.
Pr_T	Turbulent Prandtl number.
q_T	Nondimensional turbulent heat flux rate.
Re_r	Reynolds number based on reference viscosity, $Re_r = Re_\infty \mu_\infty^*/\mu_r^*(u_\infty^{*2}/C_p^*)$.
Re	Reynolds number based on free stream viscosity, $Re_\infty = \rho_\infty^* u_\infty^* L^*/\mu_\infty^*$.
t	Time.
T	Nondimensional static temperature, $T = T^* C_p^*/u_\infty^{*2}$.
u, v	Nondimensional x_1 and x_2 velocity components, $u = u^*/u_\infty^*$, $v = v^* Re_r^{1/2}/u_\infty^*$.
V	Transformed v velocity in the boundary-layer.

ORIGINAL PAGE IS
OF POOR QUALITY

x_1, x_2 Nondimensional coordinates (surface or Cartesian), $x_1 = x_1^*/L^*$, $x_2 = Re_r^{1/2}\, x_2^*/L^*$.

w Wavelength.

α u_e^2/T_e .

β Pressure gradient parameter, $(2\xi/u_e)(du_e/d\xi)$.

γ Ratio of specific heats, C_p/C_v .

$\bar{\gamma}$ Transverse intermittency function.

δ Nondimensional displacement thickness.

δ_{kinc} Incompressible displacement thickness.

δ_T Displacement body height.

ε Eddy viscosity.

$\bar{\varepsilon}$ Eddy viscosity parameter, $\bar{\varepsilon} = 1 + \frac{\varepsilon}{\mu}\Gamma$.

$\hat{\varepsilon}$ Eddy viscosity parameter, $\hat{\varepsilon} = 1 + \frac{\varepsilon}{\mu}\frac{Pr}{Pr_T}\Gamma$.

η Transformed normal variable.

θ Static temperature ratio, $\theta = T/T_e$.

θ_s Surface inclination of the body.

θ_T Surface inclination of the displacement body.

$\bar{\Theta}$ Nondimensional momentum thickness.

Γ Longitudinal intermittency function.

μ Nondimensional viscosity, $\mu = \mu^*/\mu_r^*(u_\infty^{*2}/C_p^*)$.

ξ Transformed longitudinal variable.

π_1, π_2 Functional grouping in inner region eddy viscosity model.

τ_T Nondimensional turbulent shear stress.

ρ Nondimensional density, $\rho = \rho^*/\rho_\infty^*$.

Subscripts

e Conditions evaluated on the displacement body or at the outer edge of the boundary layer.

$f.p.$ Flat plate value.

i	Index for the longitudinal finite difference mesh.
w	Conditions evaluated at the wall.
∞	Conditions evaluated in the upstream freestream.

Superscripts

*	Denotes dimensional quantities.

ORIGINAL PAGE IS
OF POOR QUALITY

INTRODUCTION

This research is concerned with the two-dimensional supersonic flow of thick turbulent boundary layers over a train of relatively small wave-like protuberances. Interest in this subject arises from the need to predict the extent to which an initially flat plate boundary layer has been disturbed by a regular corrugation in the wall surface. The flow conditions and the geometry considered here are such that there exists a strong interaction between the viscous and inviscid flow. The problem cannot be solved without including interaction effects because classical boundary layer methods would terminate in a separation point singularity.

To handle the present subject by boundary-layer methods, a technique for treatment of the interacting boundary layer equations as well as models for turbulence and for the viscous-inviscid interaction process must be available. A numerical method for addressing closed bubble separation regions was developed by Werle and Vatsa [1]. It was applied to a number of laminar separated flow problems including flow over a train of sine-wave protuberances [2]. This method uses the interacting boundary layer equations with a time-like relaxation concept which accounts for the boundary-value nature of the problem. This approach is adopted in the present study with the inclusion of the eddy viscosity model of Cebeci and Smith into the solution scheme. The present form of the numerical algorithm includes several modifications to that of the earlier work [2, 3] in order to accommodate the turbulent nature of the flow, the thick boundary layer, and the rather dramatic geometry variations of the wavy wall.

It was found that the method was capable of handling the interacting turbulent flows of present interest. Solutions were obtained for flow of thick turbulent boundary layers over a train of waves. The results are presented in terms of surface pressure, skin friction and heat transfer distributions. The predicted trends are compared with available analytical results based on small disturbance theory and with experimental data.

GOVERNING EQUATIONS

1. Boundary Layer Equations in Physical Coordinates

The suitability of the interacting boundary layer equations for describing the relatively strong streamwise variations in the boundary layer characteristics due to sudden changes in the body geometry has been, at least for the laminar case, verified earlier [1, 2]. This approach is used in the present study in which Prandtl's classical boundary layer equations are adopted with the only modification that the pressure variation was not prescribed but calculated simultaneously from a viscous-inviscid interaction model.

The boundary layer approximation in two-dimensional viscous flow problems implies that the pressure variation is assumed to occur only along one coordinate, taken in the general direction of the wall shear layer. The degree of this approximation depends on the choice of the coordinate system. While for very thin boundary layers over a corrugated wall, or thick boundary layers over a relatively flat wall, surface coordinates were suitable, (see Ref. 3) for thick boundary layers flowing over a small amplitude wavy wall, Cartesian coordinates were found to be more appropriate. Accordingly, the governing equations will first be written to apply to both the usual surface coordinates (s^*, n^*) and the Cartesian coordinates (x^*, y^*) using the notation (x_1^*, x_2^*) to denote either of these. Non-dimensional variables of order one are now defined according to the scheme

ORIGINAL PAGE IS
OF POOR QUALITY

$$x_1 = x_1^*/L^* \quad , \quad x_2 = Re_r^{1/2}\, x_2^*/L^* \tag{1a}$$

$$u = u^*/u_\infty^* \quad , \quad v = Re_r^{1/2}\, v^*/u_\infty^* \quad , \quad p = p^*/\rho_\infty^* u_\infty^{*2} \quad ,$$

$$\rho = \rho^*/\rho_\infty^* \quad , \quad T = C_p^* T^*/u_\infty^{*2} \tag{1b}$$

with $$Re_r \equiv \rho_\infty^*\, u_\infty^*\, L^*/\mu^*(u_\infty^{*2}/C_p^*) \tag{1c}$$

and u^*, v^*, p^*, ρ^* and T^* represent the mean velocities, pressure, density and temperature respectively.

The turbulent boundary layer equations in these variables are:

Continuity Equation

$$\frac{\partial}{\partial x_1}(\rho u) + \frac{\partial}{\partial x_2}(\rho v) = 0 \tag{2}$$

Momentum Equation

$$\rho\left(u\frac{\partial u}{\partial x_1} + v\frac{\partial u}{\partial x_2}\right) = \rho_e u_e \frac{du_e}{dx_1} + \frac{\partial}{\partial x_2}\left(\mu\frac{\partial u}{\partial x_2} + \tau_T\right) \tag{3}$$

Energy Equation

$$\rho\left(u\frac{\partial T}{\partial x_1} + v\frac{\partial T}{\partial x_2}\right) = -\rho_e u_e \frac{du_e}{dx_1}u + \frac{\partial u}{\partial x_2}\left(\mu\frac{\partial u}{\partial x_2} + \tau_T\right)$$

$$+ \frac{\partial}{\partial x_2}\left(\frac{\mu}{Pr}\frac{\partial T}{\partial x_2} + q_T\right) \quad , \tag{4}$$

where τ_T and q_T are the nondimensional turbulent stress and turbulent heat flux respectively.

The gas is assumed to be air with constant specific heats and constant Prandtl number, Pr = 0.72 with the perfect gas law,

State Equation

$$p = \frac{\gamma-1}{\gamma} T \tag{5}$$

Boundary Conditions

$$u(x_1, x_2) = 0$$

$$v(x_1, x_2) = 0 \qquad \text{at } x_2 = x_{2_w}(x_1)$$

$$T(x_1, x_2) = T_w(x_1)$$

and (6)

$$u(x_1, x_2) = u_e(x_1)$$

$$T(x_1, x_2) = T_e(x_1) \qquad \text{at } x_2 \to \infty$$

where $x_{2_w}(x_1)$ describes the body surface contour ($x_{2_w} = 0$ in surface coordinates, $x_{2_w} = y_w(x)$ for Cartesian coordinates).

2. Turbulence Model

To obtain closure of the system of equations (2-6), models for the turbulent stress and turbulent heat flux terms are needed. The eddy viscosity concept used in conjunction with Prandtl's mixing length hypothesis for the wall layer region is the most widely used algebraic model for turbulent stress. A well known representation is the two layer eddy viscosity model of Cebeci and Smith which has been very successful in modeling turbulence effects for flat plate boundary layers and other attached boundary layers with moderate pressure gradients. Less favorable results are obtained when using this model for strongly interacting and separated flow regions where it appears to fail conceptually.

In general turbulent quantities like the Reynolds stress are governed by transport equations, thus requiring that the turbulence history be accounted for. The eddy viscosity concept relates the Reynolds stress to only the local mean flow gradient. This corresponds to the physical idea that production of turbulence at a point due to interaction with the mean flow is cancelled by the dissipation due to its self-interaction (this is referred to as the "local equilibrium" concept). In other words, the eddy viscosity model is the solution to a truncated transport equation. In an effort to better align the predictions for separated flows with experimental data, previous investigators (see Refs. 4 and 5 for examples) have empirically modified the equilibrium eddy viscosity model to account for the history effect. Thus 'frozen', 'relaxation', and other models were devised and successfully applied in several of separated flow predictions. One of the present authors [6] also used the 'frozen' and 'relaxation' models in the interacting boundary layer equations for separated flows with no significant improvements in the predicted results over those obtained with the basic eddy-viscosity model. An alternate way to try to achieve more satisfactory results would be to model the turbulence via the turbulent transport equations, and then eventually introduce modifications which will account for the extra effects on turbulence occurring in the strongly interacting flows. This will, of course, further tax the computing times required for these calculations.

With the above mentioned limitations in mind, the basic form of the Cebeci-Smith eddy viscosity model was adapted for the

ORIGINAL PAGE IS
OF POOR QUALITY

present study where interaction effects tend to reduce longitudinal gradients and only small separation regions are encountered. Thus we take

$$\tau_T = \varepsilon \frac{\partial u}{\partial x_2} \tag{7a}$$

and relate q_T to τ_T by the turbulent Prandtl number as

$$Pr_T \equiv (\tau_T / \frac{\partial u}{\partial x_2}) / (q_T / \frac{\partial T}{\partial x_2}) \quad . \tag{7b}$$

The turbulent Prandtl number is here taken constant, $Pr_T = 0.90$. The two layer (outer and inner region) Cebeci-Smith model is then given as:

Inner Region

$$(\varepsilon/\mu)_i = \frac{\rho^* \bar{\ell}^{*2}}{\mu^*} \left| \frac{\partial u^*}{\partial x_2^*} \right| \tag{8a}$$

where $$\bar{\ell}^* = K_1 x_2^* [1 - \exp(-x_2^*/A^*)] \tag{8b}$$

with $K_1 = 0.40$ and

$$A^* = 26 (\mu^*/\rho^*) (\mu_w^* \left| \frac{\partial u^*}{\partial x_2^*} \right|_w / \rho^*)^{-1/2} \tag{8c}$$

where the absolute value of $\partial u^*/\partial x_2^*$ has been introduced in equation (8c) as a modification of the Cebeci-Smith model for reverse flows.

Outer Region

$$(\varepsilon/\mu)_o = \frac{\rho^* u_e^*}{\mu^*} K_2 \bar{\gamma} \delta_{kinc} \tag{9a}$$

where $\bar{\gamma}$ is the transverse intermittency function

$$\bar{\gamma} = \{1 - \mathrm{erf}[5(x_2/x_{2_e} - 0.78)]\}/2 \qquad (9b)$$

The variable x_{2_e} is the value of x_2 at which $u/u_e = 0.995$, and δ_{kinc} is the incompressible displacement thickness.

3. Boundary Layer Equations in Transformed Variables

The boundary layer equations given in Section 1 are here recast using the Levy-Lees transformation.

The new independent variables are defined by

$$\xi = \int_0^{x_1} \rho_e \mu_e u_e \, dx_1 \,, \qquad \eta = \frac{u_e}{\sqrt{2\xi}} \int_0^{x_2} \rho \, dx_2 \qquad (10a,b)$$

The normalized dependent variables are now defined as:

velocity ratio,

$$F = u/u_e \qquad (11a)$$

mean static enthalpy ratio

$$\theta = T/T_e \qquad (11b)$$

ORIGINAL PAGE IS
OF POOR QUALITY

or, mean total enthalpy

$$g = H/H_e \qquad (11c)$$

With these definitions, equations (2-4) become:

Continuity Equation

$$\frac{\partial V}{\partial \eta} + 2\xi \frac{\partial F}{\partial \xi} + F = 0 \qquad (12)$$

Momentum Equation

$$2\xi F \frac{\partial F}{\partial \xi} + V \frac{\partial F}{\partial \eta} = \beta(\theta - F^2) + \frac{\partial}{\partial \eta}\left(\ell \bar{\varepsilon} \frac{\partial F}{\partial \eta}\right) \qquad (13a)$$

or

$$2\xi F \frac{\partial F}{\partial \xi} + V \frac{\partial F}{\partial \eta} = \left(1 + \frac{\alpha}{2}\right) \beta(g - F^2) + \frac{\partial}{\partial \eta}\left(\ell \bar{\varepsilon} \frac{\partial F}{\partial \eta}\right) \qquad (13b)$$

Static Temperature Energy Equation

$$2\xi\, F \frac{\partial \theta}{\partial \xi} + V \frac{\partial \theta}{\partial \eta} = \alpha \ell \bar{\varepsilon} \left(\frac{\partial F}{\partial \eta}\right)^2 + \frac{\partial}{\partial \eta}\left(\ell \frac{\hat{\varepsilon}}{Pr} \frac{\partial \theta}{\partial \eta}\right) \tag{14a}$$

or

Total Temperature Energy Equation

$$2\xi\, F \frac{\partial g}{\partial \xi} + V \frac{\partial g}{\partial \eta} = \frac{2\alpha}{2+\alpha}\left[\ell(\bar{\varepsilon} - \hat{\varepsilon}/Pr) F \frac{\partial F}{\partial \eta}\right] + \frac{\partial}{\partial \eta}\left(\frac{\ell \hat{\varepsilon}}{Pr} \frac{\partial g}{\partial \eta}\right), \tag{14b}$$

where ℓ is the viscosity parameter defined by

$$\ell = \rho\mu/\rho_e\mu_e \tag{15}$$

with μ given from Sutherland's viscosity law and the turbulent parameters, $\bar{\varepsilon}$ and $\hat{\varepsilon}$ are defined as

$$\bar{\varepsilon} = 1 + (\varepsilon/\mu)\ \Gamma \tag{16a}$$

$$\hat{\varepsilon} = 1 + (\varepsilon/\mu)\ \frac{Pr}{Pr_T}\ \Gamma \tag{16b}$$

where Γ is the streamwise intermittency function: for fully laminar flow $\Gamma = 0$ and for fully turbulent flow $\Gamma = 1$, while for the transitional region its value varies smoothly from zero to one. The parameters α and β are obtained from the local inviscid flow as

$$\alpha = u_e^2/T_e \tag{17a}$$

$$\beta = \frac{2\xi}{u_e} \frac{du_e}{d\xi} \tag{17b}$$

State Equation

$$\rho_e/\rho = \Theta \tag{18a}$$

or

$$\rho_e/\rho = \frac{\alpha}{u_e^2}\left(H - \frac{u_e^2}{2} F^2\right) \tag{18b}$$

Boundary Conditions

$$\begin{aligned} F(\xi,\eta) &= 0 \\ V(\xi,\eta) &= 0 \\ \theta(\xi,\eta) &= T_w/T_e \end{aligned} \qquad \text{at} \quad \eta = \eta_w \tag{19a}$$

or $\quad g(\xi,\eta) = H_w/H_e$

where $\eta_w = 0$ for surface coordinates and $\eta_w = \eta_w(\xi)$ for Cartesian coordinates. Also we have that

$$\begin{aligned} F(\xi,\eta) &= 1 \\ \theta(\xi,\eta) &= 1 \qquad \text{as} \quad \eta \to \infty \end{aligned} \tag{19b}$$

or $\quad g(\xi,\eta) = 1$

The turbulence relations given in Section 2 can be expressed in transformed variables as:

Inner Region

$$(\varepsilon/\mu)_i = \sqrt{Re_r}\ \frac{\rho_e^2\, u_e^2\, K_1^2\, x_2^2\, \pi_1^2}{\mu_e \sqrt{2\xi}\ \ell\theta^3} \left|\frac{\partial F}{\partial \eta}\right| \tag{20a}$$

where $\quad \pi_1 = 1 - \exp(-\pi_2)$ (20b)

$$\pi_2 = \frac{x_2\, \rho_e\, u_e}{26\ell\, \theta^2 \mu_e} \left(\theta\sqrt{Re_r}\ \frac{\mu_e\, \ell_w}{\sqrt{2\xi}} \left|\frac{\partial F}{\partial \eta}\right|_w\right)^{1/2} \tag{20c}$$

Outer Region

$$(\varepsilon/\mu)_o = \frac{\rho_e\, u_e}{\mu_e} Re_r\, K_2\, \frac{\bar{\gamma}\, \delta_{kinc}}{\ell\theta^2} \tag{20d}$$

$$\delta_{kinc} = \frac{\sqrt{2\xi}}{\sqrt{Re_r}\ \rho_e u_e} \int_0^{\eta_e} \theta(1-F)\, d\eta \tag{20e}$$

ORIGINAL PAGE IS
OF POOR QUALITY

Note that, as far as the form of the governing equations is concerned, the only difference between the use of surface coordinates and Cartesian coordinates is in the wall boundary condition equation (19a). This can be eliminated using Prandtl's transposition theorem by writing that

$$\bar{\xi} = \xi \tag{21a}$$

$$\bar{\eta} = \eta - \eta_w(\xi) \tag{21b}$$

$$\bar{V} = V - 2\xi\eta_w' F \tag{21c}$$

With these transformation equations (12-14) and (19) yield:

Continuity Equation

$$\frac{\partial \bar{V}}{\partial \bar{\eta}} + 2\bar{\xi}\frac{\partial F}{\partial \bar{\xi}} + F = 0 \tag{22a}$$

Momentum Equation

$$2\bar{\xi} F \frac{\partial F}{\partial \bar{\xi}} + \bar{V}\frac{\partial F}{\partial \bar{\eta}} = \beta(\theta - F^2) + \frac{\partial}{\partial \bar{\eta}}\left(\ell\bar{\varepsilon}\frac{\partial F}{\partial \bar{\eta}}\right) \tag{22b}$$

or

$$2\bar{\xi} F \frac{\partial F}{\partial \bar{\xi}} + \bar{V}\frac{\partial F}{\partial \bar{\eta}} = \left(1 + \frac{\alpha}{2}\right)\beta(g - F^2) + \frac{\partial}{\partial \bar{\eta}}\left(\ell\bar{\varepsilon}\frac{\partial F}{\partial \bar{\eta}}\right) \tag{22c}$$

Energy Equation

$$2\bar{\xi} F \frac{\partial \theta}{\partial \bar{\xi}} + \bar{V}\frac{\partial \theta}{\partial \bar{\eta}} = \alpha\ell\bar{\varepsilon}\left(\frac{\partial F}{\partial \bar{\eta}}\right)^2 + \frac{\partial}{\partial \bar{\eta}}\left(\frac{\ell\hat{\varepsilon}}{Pr}\frac{\partial \theta}{\partial \bar{\eta}}\right) \tag{22d}$$

or

$$2\bar{\xi} F \frac{\partial g}{\partial \bar{\xi}} + \bar{V}\frac{\partial g}{\partial \bar{\eta}} = \frac{2\alpha}{2+\alpha}\left[\ell\left(\bar{\varepsilon} - \hat{\varepsilon}/Pr\right)F\frac{\partial F}{\partial \bar{\eta}}\right] + \frac{\partial}{\partial \bar{\eta}}\left(\frac{\ell\hat{\varepsilon}}{Pr}\frac{\partial g}{\partial \bar{\eta}}\right) \tag{22e}$$

Boundary Conditions

$$F(\bar{\xi},0) = \bar{V}(\bar{\xi},0) = 0$$

$$\theta(\bar{\xi},0) = \theta_w(\bar{\xi})$$

or

$$g(\bar{\xi},0) = g_w(\bar{\xi}) \tag{23a}$$

and

$$F(\bar{\xi},\infty) = 1$$

$$\theta(\bar{\xi},\infty) = 1$$

or $$g(\bar{\xi},\infty) = 1 \qquad (23b)$$

The interacting boundary layer calculations require an initial velocity and temperature profile at some station ahead of the effective interaction region (see Figure 1). This profile was obtained here from a noninteracting two dimensional laminar-transitional-turbulent boundary layer calculation by an ordinary marching technique using a prescribed pressure distribution.

4. Inviscid/Viscous Interaction Model

The interaction of the boundary layer with the isentropic supersonic inviscid flow is modeled in the pressure gradient parameter β by coupling it to the inclination θ_T. The edge pressure is obtained from the Prandtl-Meyer relation approximated here to second order in terms of θ_T as

$$p_e = \frac{1}{\gamma M^2} + \frac{\theta_T}{\sqrt{M_\infty^2 - 1}} + \frac{(M_\infty^2 - 2)^2 + \gamma M_\infty^4}{4(M_\infty^2 - 1)^2}\,\theta_T^2 \qquad (24)$$

where $$\theta_T = \tan^{-1}(d\delta_T/dx) \qquad (25a)$$

$$\delta_T = y_w + \delta \cos\theta_S \qquad (25b)$$

$$\theta_S = \tan^{-1}(dx_2/dx_1) \qquad (25c)$$

$$\delta = Re_r^{-1/2} \int_{x_{2_w}}^{\infty} \left(1 - \frac{\rho u}{\rho_e u_e}\right) dx_2 \qquad (25d)$$

ORIGINAL PAGE IS
OF POOR QUALITY

Once p_e is obtained the isentropic relations and Euler's equation are used to obtain β in equation (17b). Thus, the inviscid and viscous flows must be solved simultaneously since they are directly connected through the displacement thickness given in equation (25c).

NUMERICAL METHOD OF SOLUTION

The numerical method used is an implicit finite difference scheme written for the similarity form of the governing equations that marches from some initial station along the surface to the terminal point of interest. To account for the boundary value nature of the problem, Werle and Vatsa [1] have added the time dependent concept, similar to the one used for the solution of elliptic partial differential equations. This results in modification of only the momentum equation (22b) by replacing the pressure parameter β with $\bar{\beta}$ defined as

$$\bar{\beta} = \beta + \frac{\partial \delta_T}{\partial t} \, . \tag{26}$$

This method has been successfully applied to laminar separated flow problems with various flow configurations including one with multiple interacting regions [2, 3]. The extension of this approach to turbulent boundary layers involves, aside from inclusion of the eddy viscosity model into the solution scheme, a number of modifications (see also Ref. 6). Specifically, the following steps were taken.

1. The numerical stability and convergence rate has been enhanced by introducing a new differencing in the continuity equation. It has only recently been recognized [7, 8] that the longitudinal derivatives in the continuity equation provide a path for interacting flows to propagate information upstream. To accommodate this numerically requires the use of some sort of a forward difference procedure. In the present work we adopt in the continuity equation the following forward differencing

$$\left(\frac{\partial F}{\partial \xi}\right)_i = \frac{F_{i+1}^{(o)} - F_i}{\Delta \xi}$$

where the superscript (o) denotes values at the previous time step and subscript i refers to the ith station along the length of the surface.

2. The reliability of the present algorithm was enhanced by adopting the 'upwind differencing' concept for the longitudinal convection effects. In the reversed flow region upwind differencing was used in the longitudinal direction for the convective terms in order to satisfy the stability requirements. This eliminates the so-called 'artificial convection' concept used earlier [2] for the laminar case. This modification is significant because the velocities in the reversed flow regions are larger in the turbulent case than in the laminar. Thus the convection term in the momentum equation is differenced as

$$F_i \left(\frac{\partial F}{\partial \xi}\right)_i = \frac{1}{2}\{\tilde{F}_i + |\tilde{F}_i|\}(F_i - F_{i-1})/\Delta\xi +$$

$$+ \frac{1}{2}\{\tilde{F}_i - |\tilde{F}_i|\}(F_{i+1}^{(o)} - F_i)/\Delta\xi \quad . \qquad (27)$$

$\tilde{F}_i$ is replaced by F_{i-1} for forward flow, and by $F_i^{(o)}$ for reversed flow. By replacing the $\tilde{F}_i$ with $F_i^{(o)}$ the occurrence of a separation point singularity is avoided [1, 6]. Note that the first term on the right hand side of equation (27) vanishes for reversed flow, and the second term vanishes for the forward flow. The same procedure was followed with the term $F\partial\theta/\partial\xi$ in the energy equation.

Furthermore, the upwind differencing was found also helpful in the η direction, in the convective dominated outer regions of the thick turbulent boundary layer. It was brought to our attention* that upwind differencing of the $\partial F/\partial\eta$ term in the momentum equation might be required to satisfy the convergence criteria of the numerical scheme (see also Ref. 9). In the boundary layer near the wall the diffusion term $F_{\eta\eta}$ dominates the convective-like term F_η and a central difference scheme for F_η is appropriate. However, in the outer reaches of the boundary layer the diffusion term decreases significantly and numerical instabilities occur. From a study of the model equation $F_{\eta\eta} + \alpha F_\eta = 0$ it is found that with central differencing the criteria $|\alpha\ \Delta\eta| \leq 2$ must be adhered to, to avoid these oscillations. Hence the term F was central differenced when $|\alpha\ \Delta\eta| \leq 1$ and upwind differenced when $|\alpha\ \Delta\eta| > 1$.

3. The convergence rate of the time relaxation solution method for the thick boundary layers has been found much slower than for thin boundary layers. The two cases differ largely in that for the thick boundary layer the disturbance of the total displacement body from the flat plate value is very small. It was argued that the numerical truncation error can be of the same order as this relative change per one iteration, thus leading to very small convergence rate. We introduced therefore a new variable D_T in place of the total displacement body δ_T. The D_T is defined as $D_T \equiv [\delta_T(\xi,t) - \delta_i(\xi_i)]/h_s$, where $\delta_i(\xi_i)$ is the displacement thickness at the initial station and h_s is a constant

* R.T. Davis, Personal Communication.

ORIGINAL PAGE IS
OF POOR QUALITY

of the order of the maximum protuberance height. Calculations performed with this modification show improvement in the convergence rate.

The accuracy of the calculated solutions depends on the degree of precision of the finite-difference approximation and the step size. In turbulent boundary layers, large changes occur in the velocity profile in the inner layer very near the surface. A sufficient number of mesh points are needed near the wall in order to get a good resolution in the predictions of wall shear and surface heat transfer. At the outer edge of the boundary layer where the Levy-Lees variable η acquires large values, the changes are, on the other hand, very small. This is especially pertinent in the case of a thick turbulent boundary layer disturbed by a relatively small protuberance. Thus, for reasons of efficiency and accuracy a variable mesh size in the η direction is used in solving most turbulent boundary layers. A mesh growing in size from the wall as a geometric progression is used in the present algorithm. Blottner [10] has shown that in terms of a transformed normal variable $N(\eta)$ replacing the stretched Levy-Lees variable η, the truncation error is proportional to ΔN^2 as $N \to 0$, or the method of calculation is second order accurate. At the jth grid point the physical coordinate is obtained from

$$\eta_j = \eta_{j_{max}} (K^{N_j/\Delta N_o} - 1)/(K^{1/\Delta N_o} - 1) \qquad (28)$$

where $K = \Delta\eta_j/\Delta\eta_{j-1}$, $N_j = (j-1)\Delta N$, $(j_{max}-1)\Delta N = 1$, and where ΔN is the constant step in the transformed plane. The second order accuracy is achieved by varying j_{max} and holding ΔN_o fixed [10].

ORIGINAL PAGE IS
OF POOR QUALITY

It was found here that if instead one replaced ΔN_o by ΔN, where ΔN is of course varying with j_{max}, while holding K fixed the error diminishes with ΔN as $K^{-1/\Delta N}$, i.e. much faster than ΔN^2. Further details are given in Appendix A. Figures 2 show the surface heating parameter's dependence on ΔN and thus provides an accurate error estimation procedure. Based on this step size study it was found that with values of $\eta_{max} = 200$, $j_{max} = 55$, and $K = 1.254$, a 7% truncation error was incurred in the calculation of wall heat transfer. This represents an acceptable compromise between the accuracy and the efficiency of calculations.

The governing equations were linearized and the partial derivatives were replaced by finite differences. The eddy viscosity term ε/μ, appearing as a nonlinear term in the governing equations, is approximated by its previous station value. Central differences were used to represent partials with respect to η (except as noted above where upwind differencing for F_η was required in the outer region of the boundary layer) as well as for the streamwise derivatives of the displacement body height, δ_T. Upwind differencing was used in the convective terms in the momentum and energy equations and forward differencing with respect to ξ in the continuity equation.

The calculation commences with certain initial conditions and then through the time dependent approach [1] the steady state solution for a given set of boundary conditions is sought. In the present calculations the initial conditions were set by taking the zero time displacement body to correspond to a flat plate boundary layer and the surface protuberance to be of zero height. Subsequent time sweeps are conducted with the wave amplitude

increasing gradually by a small amount. After the desired geometry is reached (after the first 10-15 sweeps) the time-like relaxation process is continued until the flow properties are relaxed to the final value. This process is shown in Figure 3a where the skin friction coefficient at one location (s = 3.58) is shown as a function of time iteration number. This location is near the junction of the flat plate with a single sine-wave protuberance where separation occurs. The resulting skin friction and surface heating distributions are shown in Figure 3b. For this case with a thin boundary layer, the calculation was performed in surface coordinates. Figure 3a shows that once the full protuberance height is attained (11 sweeps) it takes about 50 more sweeps for the skin friction to attain its 'steady state' value. This calculation, with 41 normal grid points and 71 longitudinal grid points were performed in 5 minutes of computer time on the IBM 370-168.

RESULTS AND DISCUSSION

A major interest of the present investigation is in the numerical predictions for thick turbulent boundary layers over a wavy wall, as those in the experiments of reference [11]. The geometry and the flow conditions were therefore chosen to coincide with those given in reference [11]. The amplitude and wave length are $a^* = 0.29$ cm, $w^* = 3.66$ cm respectively. A reference length $L^* = 15.25$ cm was chosen. The base flow conditions are defined by $M_\infty = 2.53$, $Re_\infty = 10.82 \times 10^6/m$, $T_\infty = 174°K$ and $T_w/T_o = 0.81$. Henceforth, we refer to these conditions as standard flow conditions.

To obtain the present results it is first necessary to generate initial profiles at some point ahead of the first protuberance-flat plate juncture. For the standard flow conditions this station was taken at $x = 72.90$, where the initial profiles were obtained from a noninteracting calculation to correspond to the boundary layer as it develops along the wall of the UPWT Langley Wind Tunnel [11]. The details concerning the calculation of the initial profiles are described in Appendix B. The interacting algorithm was subsequently employed between this initial station and a downstream station past the last protuberance. The problem was first formulated and solved in the customary surface coordinates. It turned out that the geometry extremes make the use of the Cartesian coordinates version of the boundary layer equations more reasonable. The results of the calculations shown here were performed with a longitudinal stepsize $\Delta x = 0.02$, and a 55 point grid across the boundary layer.

ORIGINAL PAGE IS
OF POOR QUALITY

Examples from the calculated results are presented for flow over a train of up to six waves, for Mach numbers $M_\infty = 2.5$ and 3.5, for Reynolds numbers $Re_\infty = 10.82 \times 10^6/m$ and $32.46 \times 10^6/m$ and for wall to total temperature ratios $T_w/T_o = 0.40$ and 0.81.

Figure 4 shows the contour of a train of six waves, the displacement body and the viscous and inviscid pressure distributions for the standard flow conditions. The difference in the inviscid and viscous pressures dramatically shows the effect and need for interaction. The pressure is calculated from an approximation to the Prandtl-Meyer relation, accurate to second order in flow inclination angle. The inviscid pressure is calculated using the local body slope, whereas the viscous pressure is obtained by using the slope of the displacement body ($= \delta_T = y_w + \delta$). The difference in the viscous and inviscid pressure is due to the difference in amplitudes of the actual (y_w) and displacement (δ_T) body. It is interesting to observe that the viscous pressure is almost periodic even though the average displacement thickness decreases. Figure 5 shows with the distribution of pressure the corresponding distribution of surface heat transfer and skin friction at the same base flow conditions. The pressure peaks and peaks in heating occur at about the same location ahead of the body surface peak. The peak in skin friction is shifted in the opposite direction. While the pressure distribution is nearly periodic, the heating levels and the skin friction peaks rise in the downstream direction. The rate of rise in peak heating is decreasing very slowly. These results are in contradistinction to our similar

study [3] of thin laminar flow over a train of sine-waves, where the peaks in heating decreased rapidly in the streamwise direction. Figure 6 points out the fact that the local value of the surface parameters is almost unaffected by the presence of additional downstream disturbance for turbulent boundary layers (compare also Figures 5 and 6). Simply, downstream waves have little upstream influence and the problem seems localized. Heating levels aft of waves grow as the number of waves increases, but the downstream skin friction is unaffected by the number of waves.

To demonstrate the effect on surface properties due to Mach number, wall temperature, and Reynolds number, three additional cases are shown in Figures 7A,B through 9A,B. The increase of Mach number (Figures 7A,B) from 2.5 to 3.5 causes a decrease in the ratio of $h_{max}/h_{f.p.}$. As in the standard flow case, the location which the first wave was placed was chosen in such a way that the flat plate boundary layer displacement thickness was about the same as in the experimental study of reference [11].

The lowering of wall temperature to $T_w/T_o = 0.40$ (Figures 8A,B) shows a similar trend in $h_{max}/h_{f.p.}$ as for the increase in Mach number. But the absolute rate of surface heating is much higher than in the previous case. Interestingly, the $h/h_{f.p.}$ curve is smoother here than in other cases.

Lastly, an increase in Reynolds number, shown in Figures 9A,B is seen to cause a slight increase in the ratio of peak heating.

ORIGINAL PAGE IS
OF POOR QUALITY

An interesting aspect of the present results is the location of the peaks in pressure, heat transfer and shear. The present predictions show the peaks in pressure and heating to occur at about the same location. This is in agreement with experimental observations [11]. The location of the peak pressure in the present results is shifted to the right of the location of the inviscid peak pressure location (at $y \approx 0$) by a phase angle of about 60°. Theoretical studies by Inger and Williams [12] and by Lekoudis et al. [13] predict such a shift. Data from these studies given up to $M_\infty = 2.0$ show a shift to the left which drops off quickly towards zero at $M_\infty \approx 2$. It is therefore possible to expect a phase angle in the opposite sense for $M_\infty > 2$, as is the case in present results. The maximum wall shear location obtained from present calculations is shifted to the right of the peaks in pressure and surface heating by about 60°. According to theoretical predictions [13] qualitatively such a shift is expected. Experimental data available at the same flow conditions [11] show a periodic trend in surface pressure as well as in the surface heating distribution. The periodic trend in surface pressure is observed also in the present predictions. Pressure and heating distributions between the second and third peak are compared to the experimental data [11] for Mach numbers 2.5 and 3.5 in Figure 7B. While the heating distributions in the experiments of reference [11] are nearly repetitive over consecutive waves, the present predictions show a continuous increase over the length of the waves. Note

though that in the experimental study there is also indication that separation occurs, while a lack of separation is observed in the analytical results of Figure 5. The cause of this disagreement is not certain but it could well be due to our choice of turbulence model or in the fact that the present calculations do not simulate well enough all the test conditions (three-dimensional effects or boundary layer development on the tunnel wall). Note the calculated boundary layer displacement thickness of the initial profile at station x = 72.90 is 2.86 cm, close to the value given in reference [11]. However the predicted surface heating value at this station is too high when compared to experimental data of reference [11] (The predicted value is $h_{f.p.}$ = 96.5 watts/m^2 °K vs 62.5 watts/m^2 °K in experiments). Other prediction methods also typically over predict to about the same level the heat transfer rates for boundary layers developing along the wind tunnel walls [14] thus indicating that some final adjustments may be needed in the turbulence model for these flows.

While the present prediction method has in a certain way accounted for the boundary layer displacement effect by using the interacting boundary layer equations, the effect of surface curvature was neglected. The curvature effect in turbulent flows has been summarized in a comprehensive monograph by Bradshaw [15]. It has been found that even in cases when the longitudinal surface curvature is accounted for in the governing equations the predicted surface aerodynamic parameters (surface heating, wall shear) still deviate considerably from the experimental data. Apparently, the streamline curvature has an

effect on the turbulence structure not included in the existing turbulence models. Bradshaw therefore proposed a simple correlation scheme applicable to turbulent flows with not too large streamline curvature. For the simplest equilibrium model used in the present work this correction consists of multiplying the mixing length by a factor $f = 1 + \alpha e/(\partial u/\partial y)$, where $e = \partial v/\partial x$ is the extra rate of strain induced by the streamline curvature (and $\partial u/\partial y$ is the mean rate of strain). This correction is recommended for only $0.5 \leq f \leq 1.5$. The constant α is of order 10. Because of the time lag between the first appearance of the curvature and its full effect on turbulence the effective value of αe is calculated from the lag equation

$$10\delta \frac{d}{dx} (\alpha e)_{eff} = \alpha_o e - (\alpha e)_{eff} \qquad (29)$$

where δ is the boundary-layer thickness, and the constant α_o is taken to be 10. This idea has been implemented here for the standard test case by evaluating $\partial v/\partial x$ along a streamline at each station x. It was then assumed that this is a representative value for all values of y at this station. The δ was taken to correspond to station x = 73.20. The case with base flow conditions was recalculated. It was found that a streamline had to be chosen in the lower part of the inner layer (passing the 21st grid point at x = 73.20) in order not to violate the condition $0.5 \leq f \leq 1.5$. The results of this calculation are shown in Figures 10A,B. Observe that the peaks in $h/h_{f.p.}$ and C_f are now lower and slightly dropping along the wall. A comparison between the detailed distribution of the surface

heating calculated with and without the curvature correction, and against the experimental data is shown in Figure 10b. The comparison with experiments is now more favorable on the compression side of the wave. Recall however that in the wind tunnel tests the boundary layer was separated.

To examine the effect of separation on the character of the heating distribution and also to demonstrate the capability of the method to solve multiple separation regions, calculations without curvature correction were performed with the base flow conditions but for a boundary layer developed along a flat plate up to the junction point $x = 24.30$ (Figures 11A,B). It is noticed (Fig. 11B) that when compared to the unseparated case, the heating values are lower on the expansion side of the wave. Flow separation occurred in this case due to the different history and also because of the larger pressure gradients: the ratio δ/a is here smaller than for the standard case and therefore the slope of the total displacement body steeper. This is even more apparent for a relatively very thin boundary layer. Figure 12 shows the results from a calculation performed at the same flow condition as in Figure 11, except that junction of the flat plate and the first protuberance was moved forward to $x = 3.3$ and the wave height was reduced to one-half of the previous value. Larger pressure gradients and separation regions now appear closer to the center of the valleys are observed. Again, the peak heating rates grow in the streamwise direction.

In reference [11] it was found that unlike for thin boundary layers, the peak heating rates were insensitive to the wave amplitude. To examine this question a set of calculations were performed for different ratios of wave amplitude to wave length, a/w. According to the present predictions the heating rates change considerably with the amplitude even for the thick boundary layers (Figs. 13A,B). For both thick and thin boundary layers the peak heating values, $(h/h_{f.p.})_{max}$, are plotted in Figure 14. The present predictions show similar behavior for both thin and thick boundary layers: a stronger than linear increase in peak heating with the increase of wave amplitude. Note that the curvature effect on turbulence was not accounted for in the results shown in Figures 13 and 14. The larger curvatures corresponding to higher amplitude waves probably amplify the predicted trend observed in Figures 13 and 14.

CONCLUSIONS

A numerical method capable of handling multiple interacting flow regions was adapted to the problem of thick turbulent boundary layer over a wavy wall.

The results of calculations presented in terms of surface pressure, skin friction, and heat transfer distributions disclose features distinctly different from the laminar case. The present results show a shift in the location of the viscous pressure peaks relative to the peaks in the inviscid pressure and to the peaks in the wall shear. These phase shifts are in qualitative agreement with theoretical predictions based on small disturbance theory. The location of peaks in viscous pressure and heat transfer coincide, and the longitudinal pressure variation is periodic. This is in agreement with the experimental data. The experiments also show periodicity in surface heating distribution, while the present results predict a continuous increase in heating indicating a possible weakness in the turbulence model for a surface with rapidly varying curvature. A semi-empirical modification of the eddy viscosity model, intended to account for the longitudinal curvature effect, aligns the predictions closer to the experimental data. It is recommended that future work be carried out with a more accurate turbulence model, and that a more optimal coordinate system be adopted for this problem.

ORIGINAL PAGE IS
OF POOR QUALITY

REFERENCES

1. Werle, M.J. and Vatsa, V.N., "A New Method for Supersonic Boundary Layer Separations," AIAA Journal, November 1974, pp. 1491-1497.

2. Werle, M.J., Polak, A., Vatsa, V.N., and Bertke, S.D., "Finite Difference Solutions for Supersonic Separated Flows," appearing in Flow Separation, AGARD CP 168, 1975.

3. Polak, A., Werle, M.J., Vatsa, V.N. and Bertke, S.D., "Numerical Study of Separated Laminar Boundary Layers Over Multiple Sine-Wave Protuberances," J. of Spacecraft and Rockets, Vol. 13, No. 3, March 1976, pp. 168-173.

4. Shang, J.S. and Hankey, W.L., Jr., "Numerical Solution for Supersonic Turbine Flow Over a Compressible Ramp," AIAA Journal, Vol. 13, October 1975, pp. 1368-1374.

5. Horstman, C.C., Hung, C.M., Settles, G.S., Vas, I.E., and Bogdonoff, S.M., "Reynolds Number Effects on Shock-Wave Turbulent Boundary Layer Interactions - A Comparison on Numerical and Experimental Results," AIAA Paper No. 77-42, presented at the AIAA 15th Aerospace Sciences Meeting, January 24-26, 1977, Los Angeles, California.

6. Werle, M.J. and Bertke, S.D., "Application of an Interacting Boundary Layer Model to the Supersonic Turbulent Separation Problem," Report No. AFL 76-4-21, August 1976, Dept. of Aerospace Engineering, University of Cincinnati, Cincinnati, Ohio.

7. Davis, R.T. and Werle, M.J., "Numerical Methods for Interacting Boundary Layers," Proceedings from the 25th Heat Transfer and Fluid Mechanics Institute, University of California, Davis, California, June 21-23, 1976.

8. Davis, R.T., "Numerical and Appriximate Solution of the High Reynolds Number Small Separation Problem," Advances in Engineering Sciences, Vol. 4, pp. 1451-1465, NASA CP-2001, Annual Meeting Society of Engineering Science, Hampton, Virginia, Nov. 1-3, 1976.

9. Blottner, F.G., "Computational Techniques for Boundary Layers," AGARD Lecture Series No. 73, Computational Methods for Inviscid and Viscous Two- and Three-Dimensional Flow Fields, February 1975, pp. 3-1 - 3-51.

10. Blottner, F.G., "Variable Grid Scheme Applied to Turbulent Boundary Layers," Computer Methods in Applied Mechanics and Engineering, 4 (1974), pp. 179-194.

11. Brandon, A.J., Masek, R.V. and Dunavant, J.C., "Aerodynamic Heating to Corrugation Stiffened Structures in Thick Turbulent Boundary Layers," AIAA Journal, Vol. 13, No. 11, 1975.

12. Inger, G.R. and Williams, E.P., "Subsonic and Supersonic Boundary-Layer Flow Past a Wavy Wall," AIAA Journal, Vol. 10, No. 5, May 1972, pp. 636-642.

13. Lekoudis, S.G., Nayfeh, A.H. and Saric, W.S., "Compressible Boundary Layer Over Wavy Walls," The Physics of Fluids, Vol. 19, No. 4, April 1976, pp. 514-519.

14. Couch, L.M. and Stallings, R.L., Jr., "Heat Transfer Measurements on a Flat Plate with Attached Protuberances in a Turbulent Boundary Layer at Mach Numbers of 2.49, 3.51, and 4.44," NASA TND-3736, December 1966.

15. Bradshaw, P., "Effects of Streamline Curvature on Turbulent Flow," AGARDograph No. 169 (1973).

ORIGINAL PAGE IS
OF POOR QUALITY

APPENDIX A

GRID SIZE EFFECT ON ACCURACY

The objective is to assess the accuracy of the predicted surface boundary layer characteristics from the standpoint of the normal mesh size. The very thick turbulent boundary layer as produced on the wall of the UPWT Langley tunnel is of interest here. The boundary layer calculation is carried out as an non-interacting 2-D laminar-transitional-turbulent boundary layer. The corresponding pressure gradient is calculated from the Mach number distribution given in Appendix B.

The free stream conditions in the test section are: M_∞ = 2.535, $Re_\infty/cm = 1.08 \times 10^5$, $T_\infty = 314°R$, $T_w/T_o = 0.81$ and p_∞ = 199 psf. And Pr = 0.72, $Pr_T = 0.9$ were taken. The calculation commences at s = 0.3 with a laminar boundary layer, which becomes fully turbulent at s = 2.1 ($\Delta s = 0.1$). The Mach number becomes constant at s = 40.60. The implicit finite-difference method (Flügge-Lotz-Blottner-Davis) with non-uniform grid size, varying according to a geometric progression law, is employed.

The truncation error in this type of calculation is proportional to the quantity $(\eta_{j+1} - 2\eta_j + \eta_{j-1}) \equiv \Delta\eta_j - \Delta\eta_{j-1}$, and therefore in general not second order accurate. Blottner has shown [10] that in terms of a transformed variable, $N = N(\eta)$, where the coordinate N is obtained by coordinate stretching such that ΔN is uniform, the error is of order ΔN^2. Blottner substantiates his conclusion by a set of calculations using the transformation

$$\eta_j = \eta_J (K^{N_j/\Delta N_o} - 1)/(K^{1/\Delta N_o} - 1) ,$$

where $j = 1, 2, \ldots, J = j_{max}$ = number of grid points, $N_j = (j-1)/(J-1)$, $K = \Delta n_j/\Delta n_{j-1}$, and ΔN_o = constant.

A similar type of transformation, corresponding to the geometrical variation of Δn_j is also employed here:

$$n_j = n_J (K^{N_j/\Delta N} - 1)/(K^{1/\Delta N} - 1)$$

where $\Delta N = 1/(J-1)$ and $K = K_o$ (= 1.12) does not vary with J.

Since the local truncation error is

$$E_j \equiv n_{j+1} - 2n_j + n_{j-1} = \left(\frac{\partial^2 n}{\partial N^2}\right) \Delta N^2 + 0(\Delta N^4)$$

and $$\partial^2 n/\partial N^2 = \frac{n_J}{K_o^{1/\Delta N} - 1} \left(\frac{1}{\Delta N} \ln K_o\right)^2 K_o^{N_j/\Delta N} ,$$

we get

$$E_j \sim (\ln K_o)^2 K_o^{N_j/\Delta N} n_{max}/(K_o^{1/\Delta N} - 1) .$$

At a fixed grid location j ($N_j/\Delta N = j-1$), and for a large $1/\Delta N$ the error should be therefore plotted versus $K^{-1/\Delta N}$.

A set of calculations was carried out with J = 80, 85, 90, 95, 100, 125 and 150 for K_o = 1.12 and two values of n_J (n_J = 352 and 200). For the station s = 54.0 (a location on the straight section of the tunnel wall) the wall heat transfer parameter $(\partial g/\partial n)_w$ is shown in Figure 2A. As the error term suggests, the error decreases with decreasing of n_{max}, and plots linearly with $K^{-1/\Delta N}$ as $\Delta N \to 0$. It is also observed that the two point formula [10] (used in conjunction with

ORIGINAL PAGE IS
OF POOR QUALITY

the governing equations evaluated at the wall) for evaluating $(\partial g/\partial \eta)_w$ gives better results, especially at the excessive value of η_{max}.

In a second set of calculations the value of K was varied together with J in a specified way:

$$K = K_o^m \quad ; \qquad (J-1)m = J_o - 1 \quad .$$

Here $K_o = 1.12$, m = positive integer, $J_o = 109$, $\eta_J = 200$. We take m = 1, 2, 3 or 4, so that J = 109, 55, 37 or 28. Then,

$$\eta_j = \eta_J (K_o^{mN_j/\Delta N} - 1)/(K_o^{m/\Delta N} - 1),$$

$$\Delta N = 1/(J-1) = m/(J_o-1) = m\Delta N_o$$

$$\eta_j = \eta_J (K_o^{(J_o-1)N_j} - 1)/(K_o^{1/\Delta N_o} - 1) \quad .$$

Thus the transformation is independent of ΔN and the error term, as in reference [10], is now proportional to ΔN^2. This is exhibited in Fig. 2B where the variation of the surface heat transfer parameter at station s = 54.0 is plotted for values J = 109, 55, 37 and 28 (compare with Figure 2a). These calculations were performed by first setting $K_o = 1.12$ and $J = J_o = 109$ for $0.3 \leq s \leq 44.3$. At s = 44.3, every 2nd, 3rd or 4th grid point value was used (corresponding to m = 2, 3 or 4) and the calculation marched (with the new value J = 55, 37 or 28 and $K = K_o^m$) past station 44.3.

In summary, Blottner's interpretation of the accuracy of the variable grid size was extended by showing that the error term of the numerical scheme varies linearly with the inverse square of the number of grid spacings, (J-1), when K and J are varying in a specified way, but also plots linearly with the inverse exponential of (J-1) when K is fixed.

APPENDIX B

INITIAL PROFILES FOR THICK BOUNDARY LAYERS

A major aim of the present research project was to align numerical predictions for flow of thick turbulent boundary-layers over a wavy wall with the experimental program of reference [11]. For this reason a set of calculations were first performed for the boundary layer as it develops along the wall of the UPWT Langley Tunnel. The boundary-layer calculation was carried out as a non-interacting two-dimensional laminar-transitional-turbulent boundary-layer developing from ahead of the nozzle throat under a favorable pressure gradient. In the supersonic region downstream of the throat the pressure distribution was calculated from the sidewall Mach number distribution, using isentropic relations. The Mach number distribution was obtained from a characteristics net. From these data a cubic representation for M was assumed of the form

$$M = M_T - K_1 \left(1 - \frac{s}{s_T}\right)^2 \left(1 - K_2 \frac{s}{s_T}\right) \quad ,$$

where M_T = test section Mach number at $s = s_T$. The above polynomial representation satisfies the condition $dM/ds = 0$ at $s = s_T$. At the location s_α of the first characteristic near the throat the Mach number was estimated to be $M_\alpha = 1.11$. The measured distance along the wall from s_α to s_T is 39.6 ($\sim$ 20 ft). At a location s_β, 8.86 units downstream of s_α, the Mach number is $M_\beta = 1.84$. Letting $s_\alpha = 1$, $s_\beta = 9.86$ and $s_T = 40.6$. Using

these values, the constants K_1 and K_2 can be determined. For K_1, $K_2 > 0$ and $K_2 \leq 1$ (which is the case here) the polynomial representation given above yields monotomically increasing Mach number. The subsonic-transonic section of the tunnel was also assumed to be represented by a cubic polynomial

$$M = M_i + C_1 \left(1 - \frac{s}{s_i}\right)^2 \left(1 - C_2 \cdot \frac{s}{s_i}\right) \quad ,$$

with the following properties:

ORIGINAL PAGE IS
OF POOR QUALITY

At $s = s_i = 0.3$, $M = M_i$ and $dM/ds = 0$.

At $s = s_\alpha$, $M = M_\alpha = 1.11$ and $\frac{dM}{ds} = \left(\frac{dM}{ds}\right)_{s_{\alpha_+}}$.

Three different values for M_i were chosen: 0.01, 0.03 and 0.05. It turned out that the boundary layer development downstream of the throat was not sensitive to these initial values. Taking $M_i = 0.03$, a boundary layer calculation was performed for $0.3 \leq s \leq 97.4$ with boundary layer profiles punched on IBM cards. (At $s = 40.6$ the Mach number becomes constant on the side wall; at $s \simeq 50.6$ the straight section begins.) These profiles were used as initial data for the interacting thick turbulent boundary layers. The table below gives the calculated boundary layer displacement thickness distribution along the constant Mach number section of the UPWT Langley tunnel wall at ten stations, for $M_T \equiv M_\infty = 2.53$, $T_\infty = 174.4°K$, $T_w/T_o = 0.81$, $Re_\infty = 10.82 \times 10^6/m$, $Pr = 0.72$ and $Pr_T = 0.90$.

s	40.6	44.6	48.6	52.6	56.6	60.6	64.6	68.6	72.6	76.6
δ^* (cm)	1.69	1.84	1.98	2.12	2.26	2.40	2.54	2.67	2.80	2.93

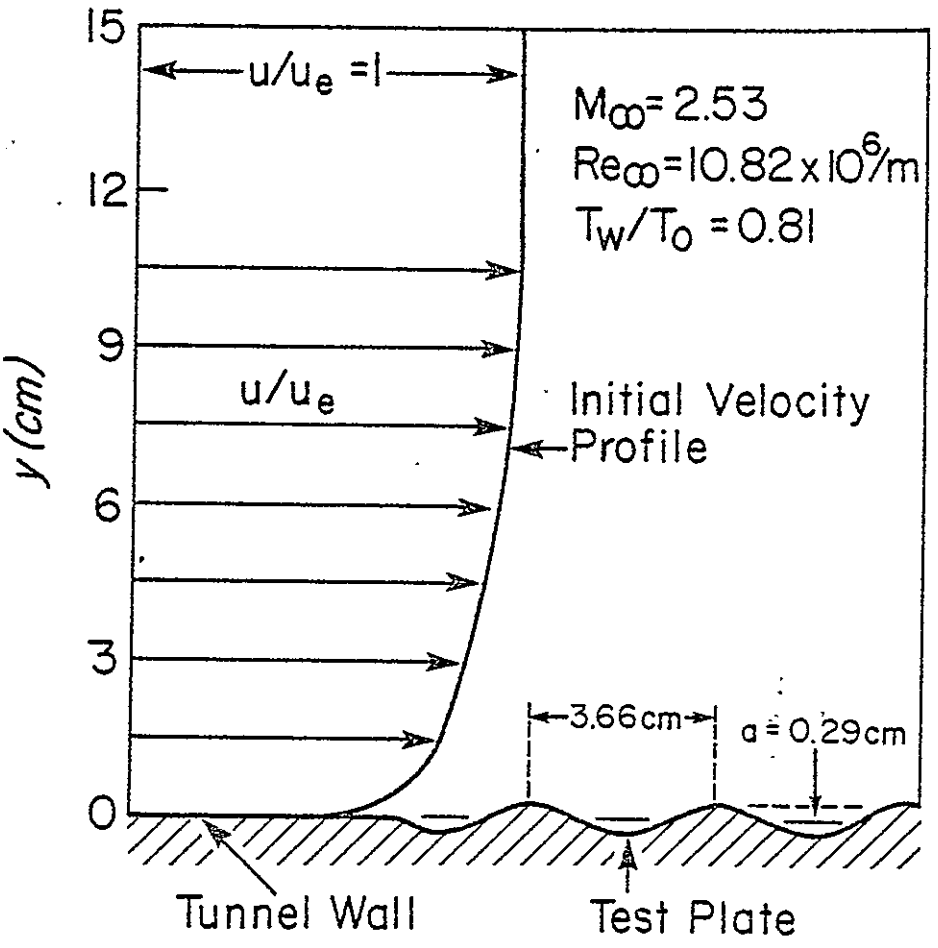

Figure 1 FLOW GEOMETRY

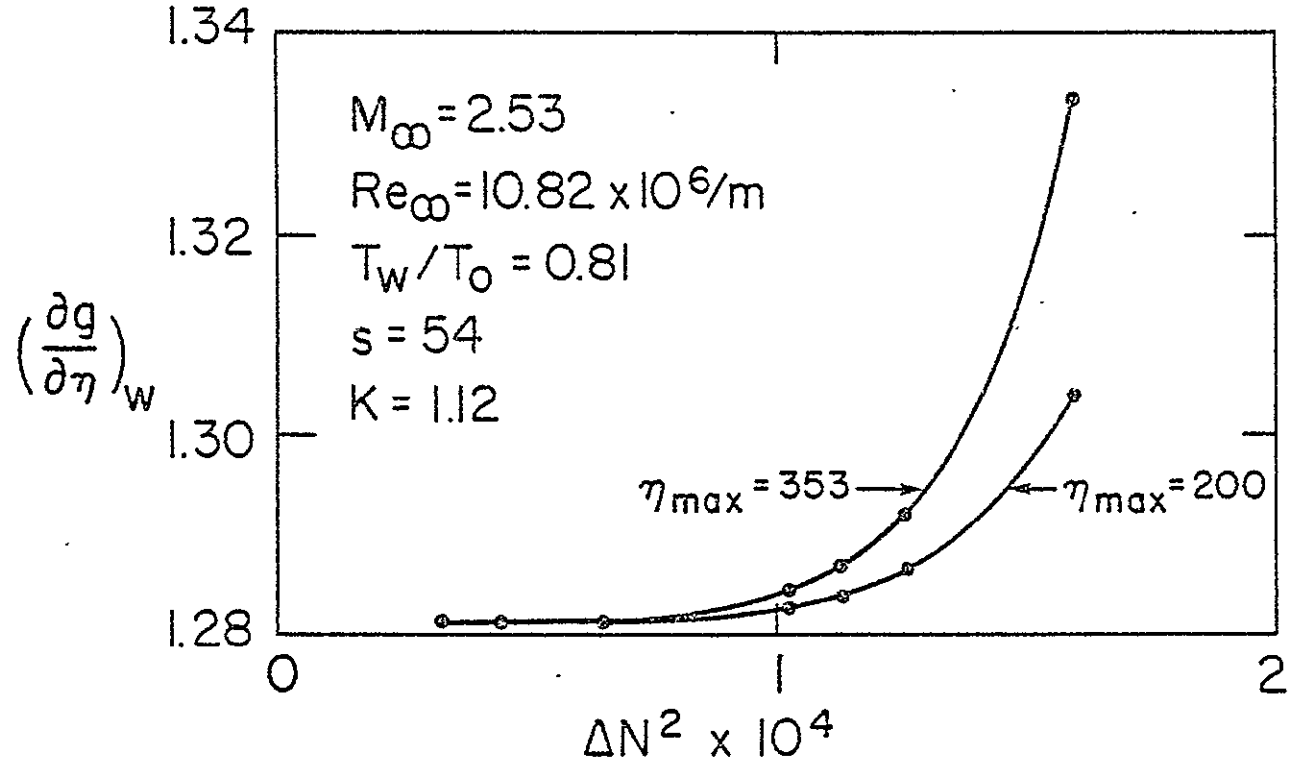

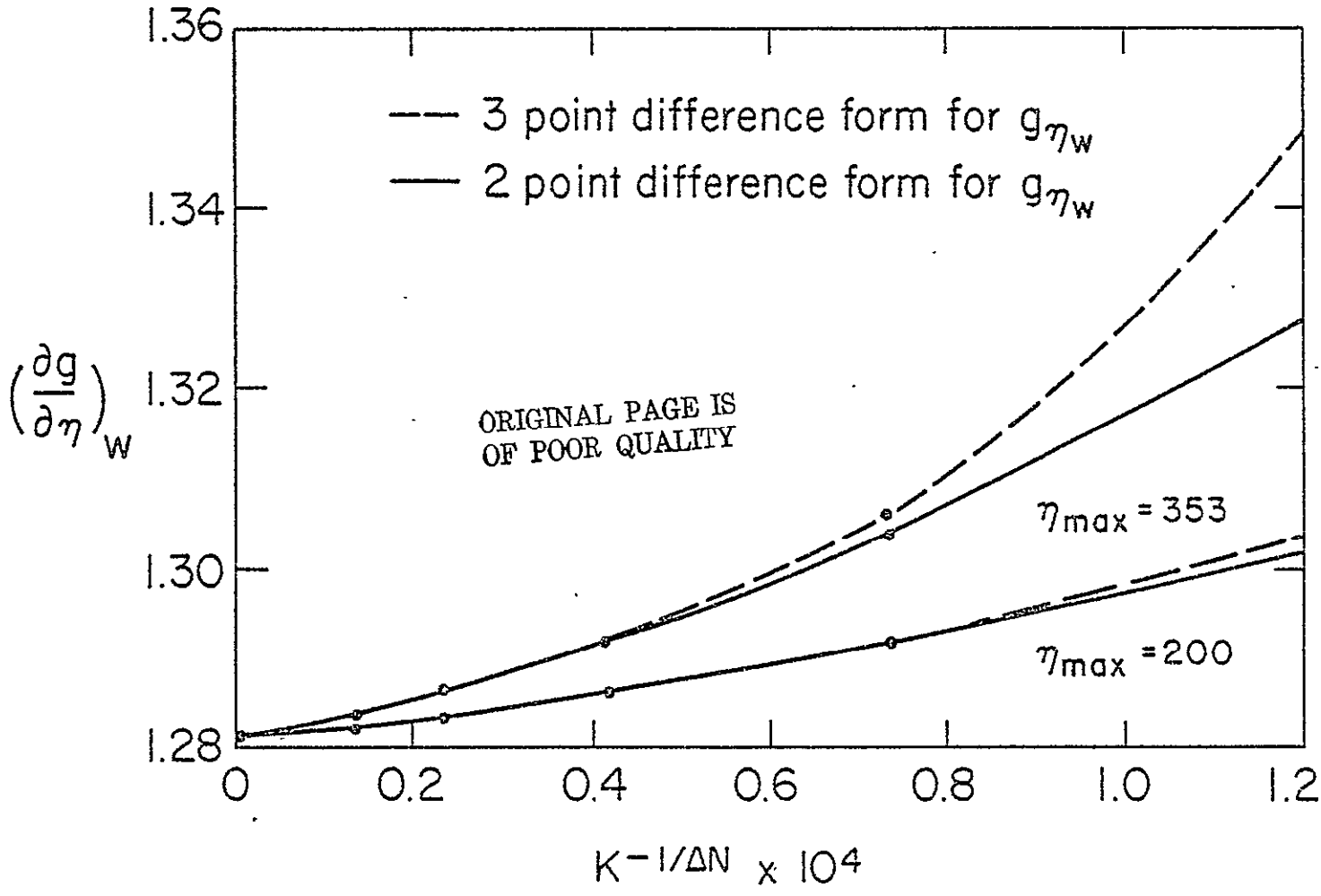

Figure 2A ACCURACY STUDY OF WALL HEATING LEVEL

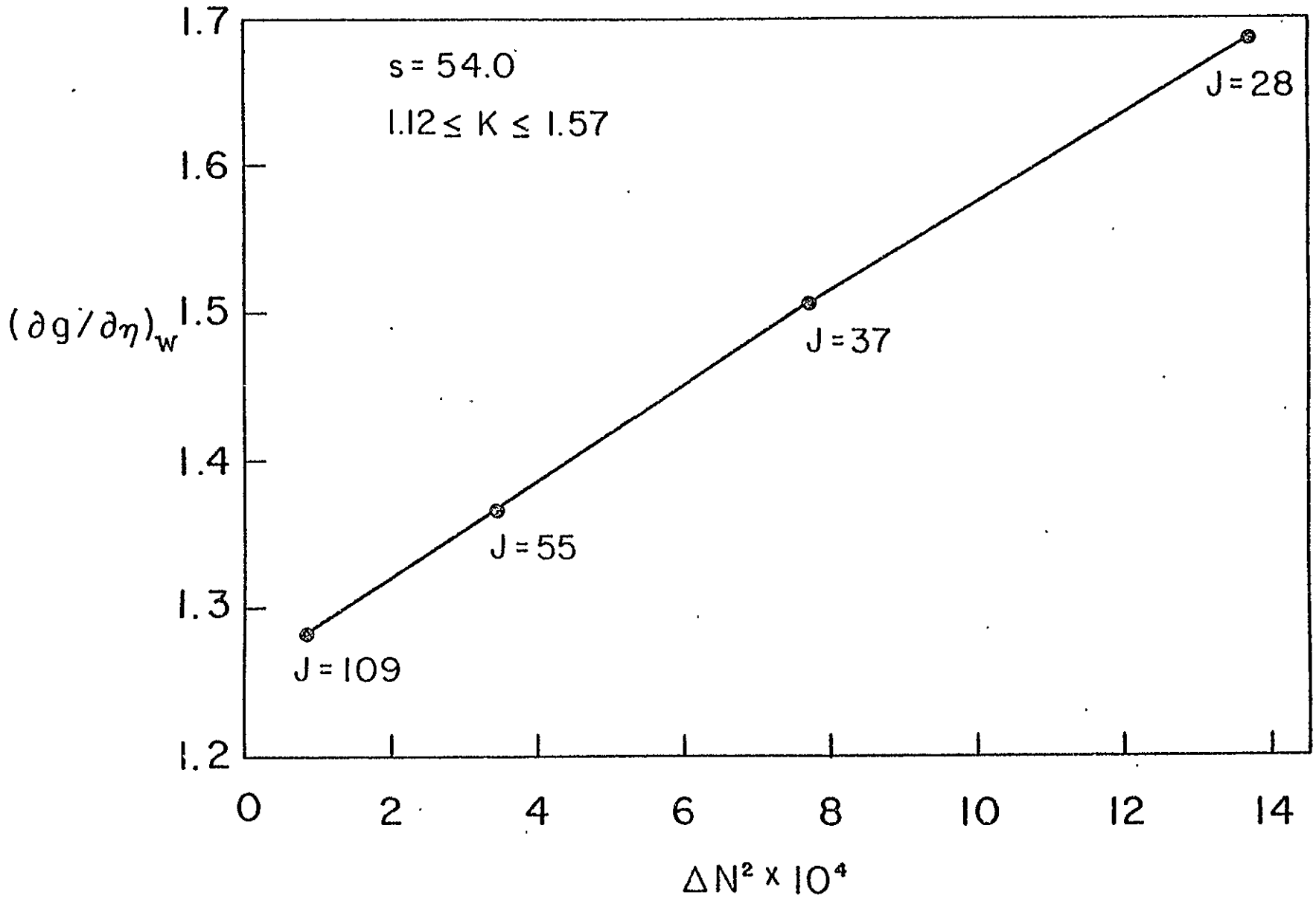

Figure 2B ACCURACY STUDY OF WALL HEATING LEVEL

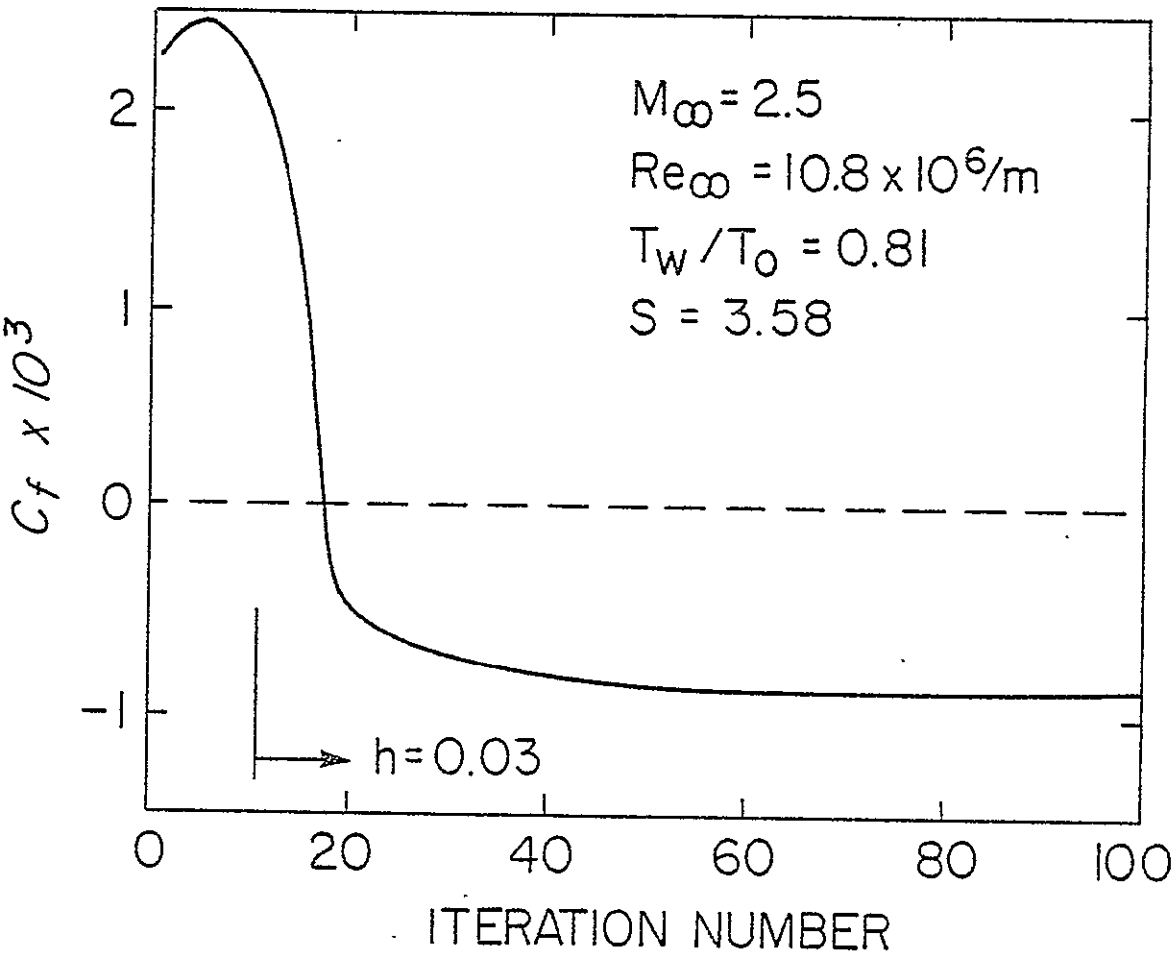

Figure 3A CONVERGENCE PROPERTY OF SKIN FRICTION

ORIGINAL PAGE IS
OF POOR QUALITY

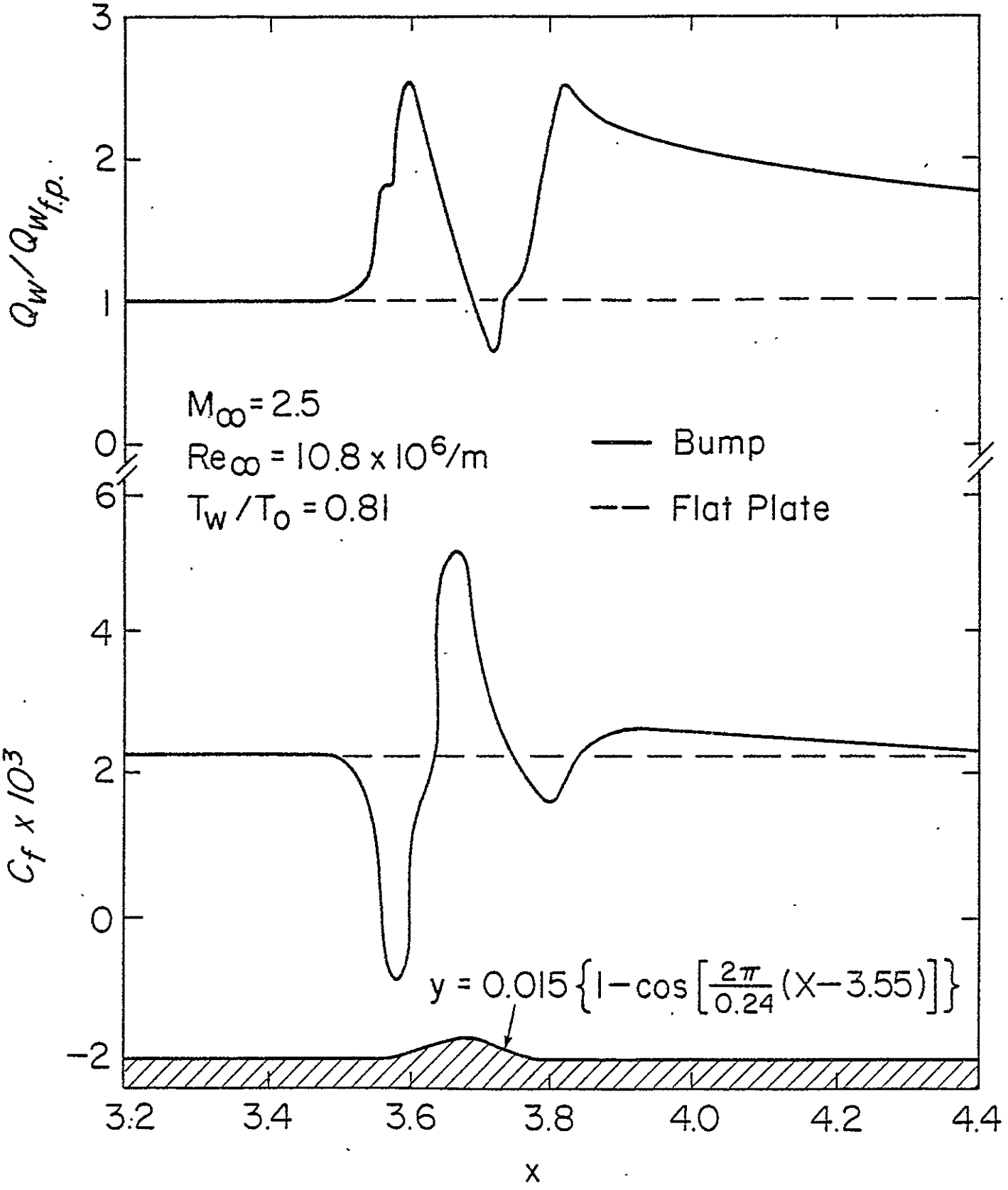

Figure 3B SURFACE PROPERTIES FOR ONE PROTUBERANCE

ORIGINAL PAGE IS
OF POOR QUALITY

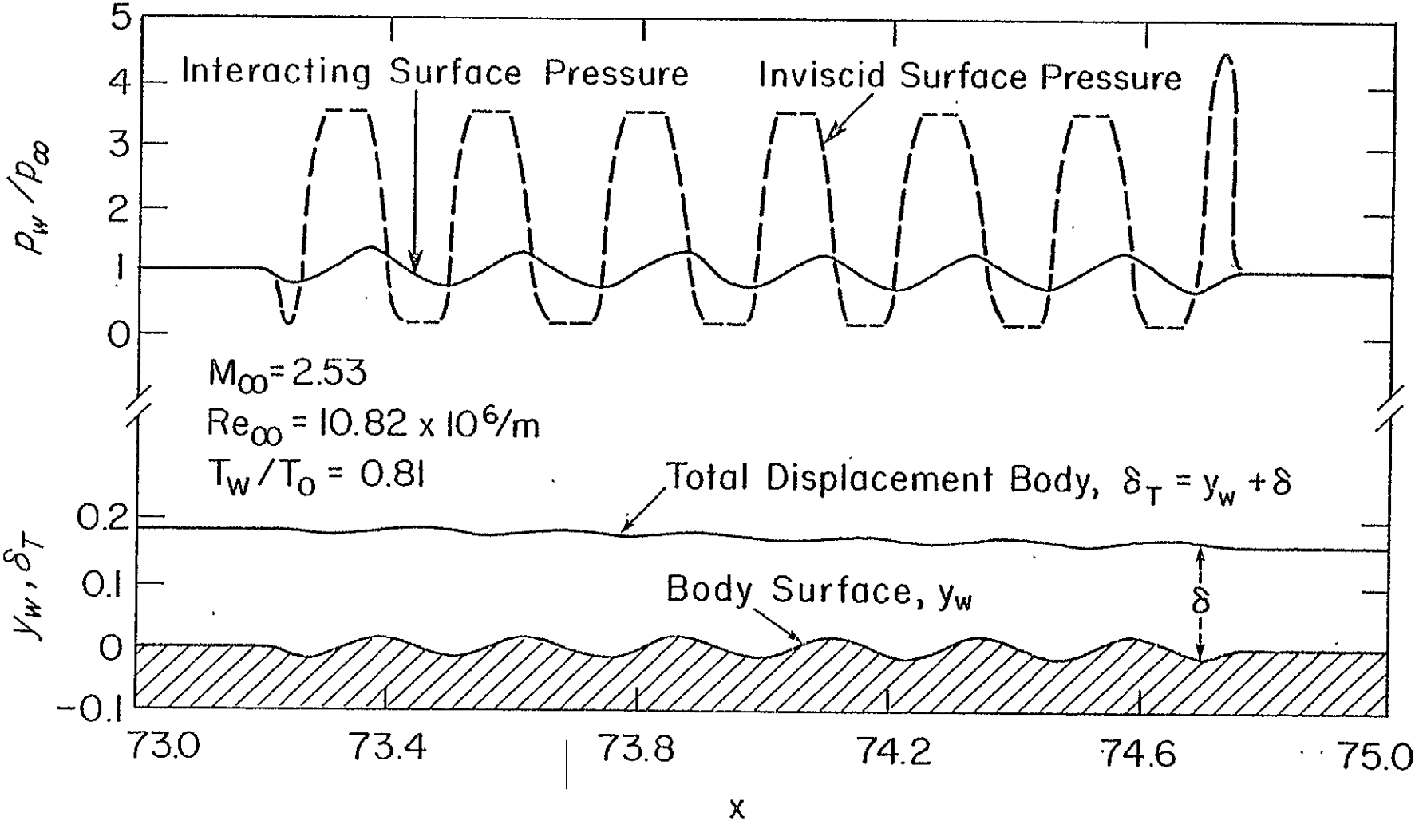

Figure 4 DISPLACEMENT BODY AND SURFACE PRESSURE – STANDARI CASE

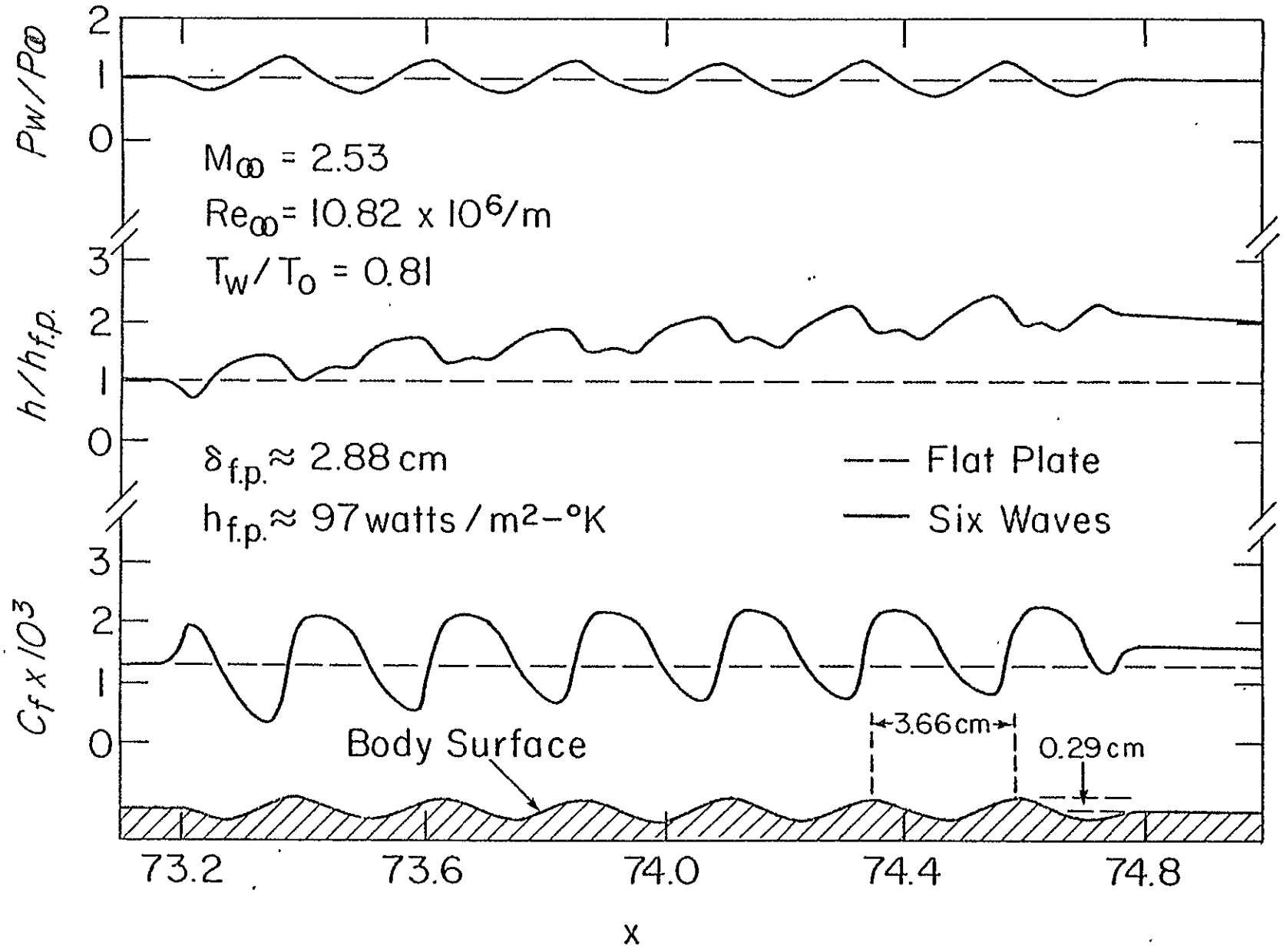

Figure 5 SURFACE PROPERTIES – STANDARD CASE

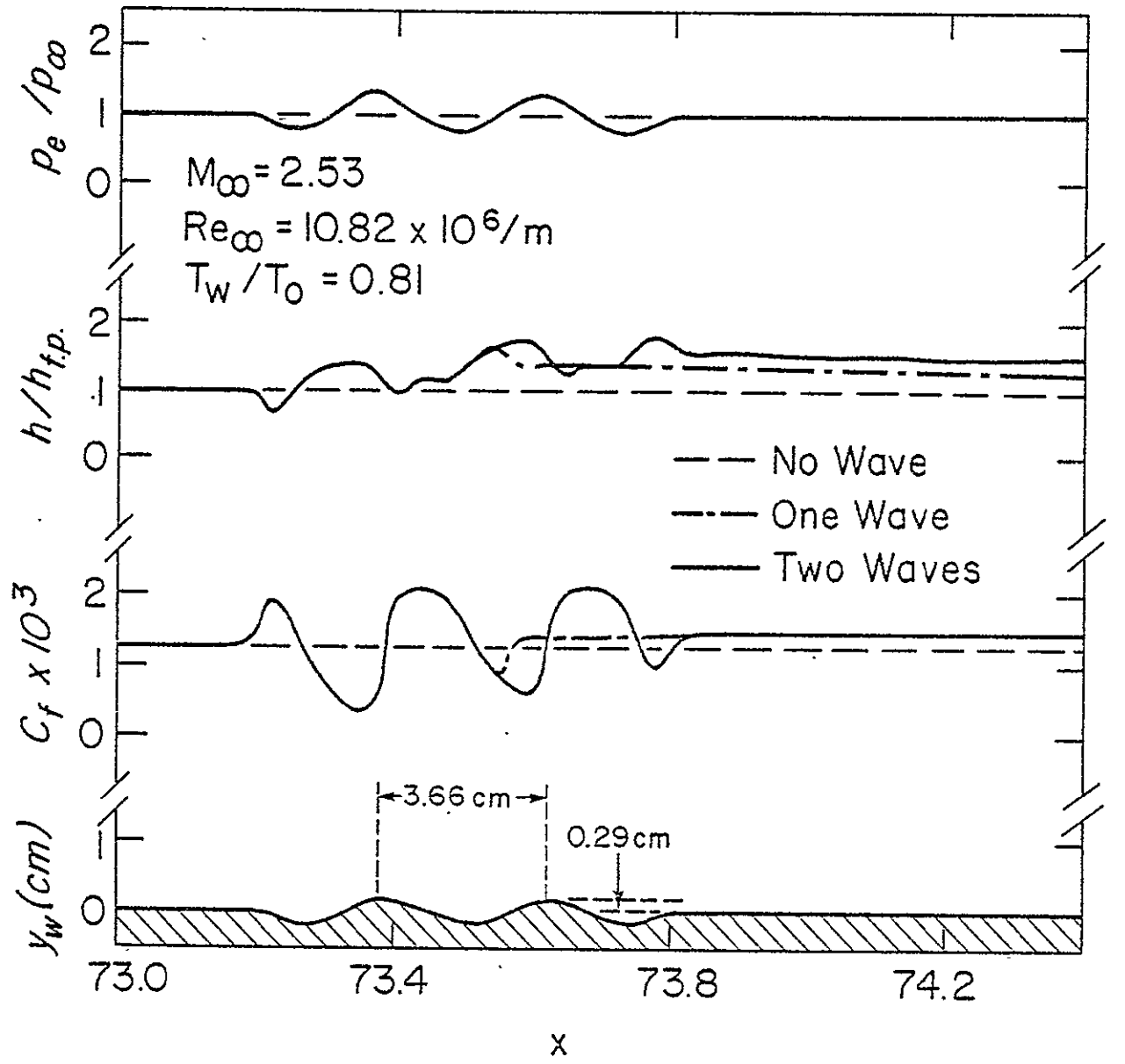

Figure 6 DOWNSTREAM EFFECT ON SURFACE PROPERTIES

ORIGINAL PAGE IS
OF POOR QUALITY

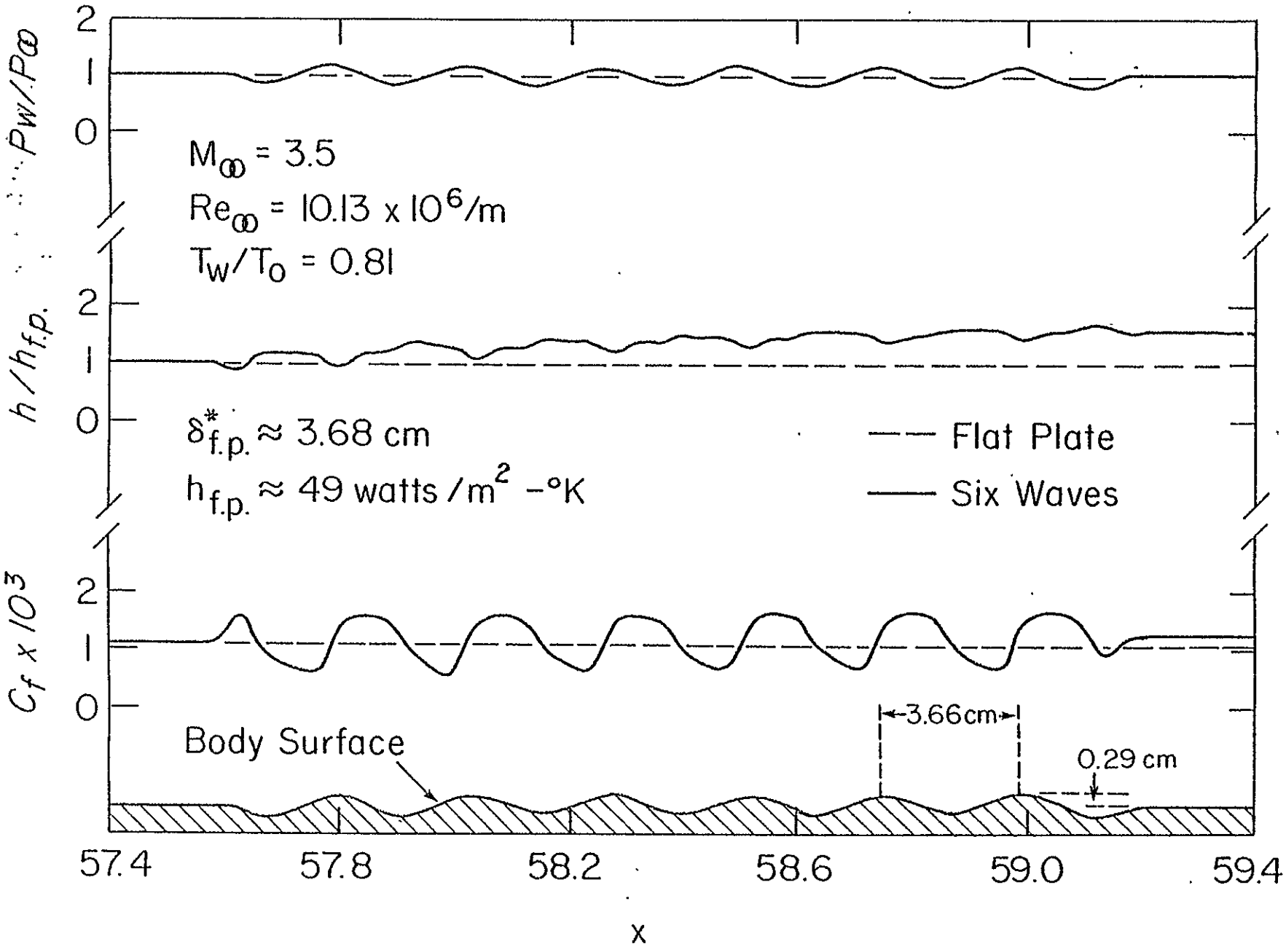

Figure 7A MACH NUMBER EFFECT ON SURFACE PROPERTIES

ORIGINAL PAGE IS
OF POOR QUALITY

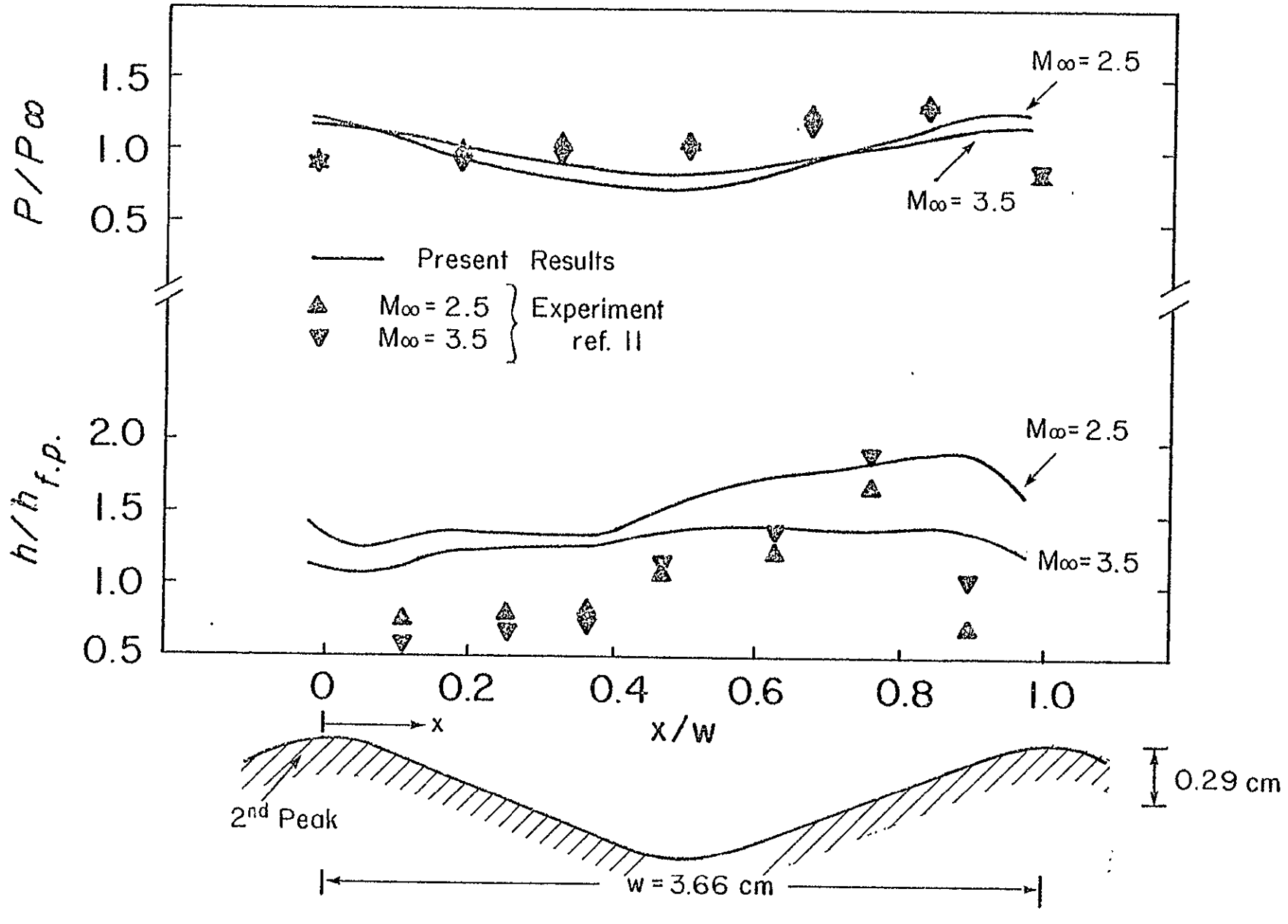

Figure 7B MACH NUMBER EFFECT ON SURFACE PROPERTIES

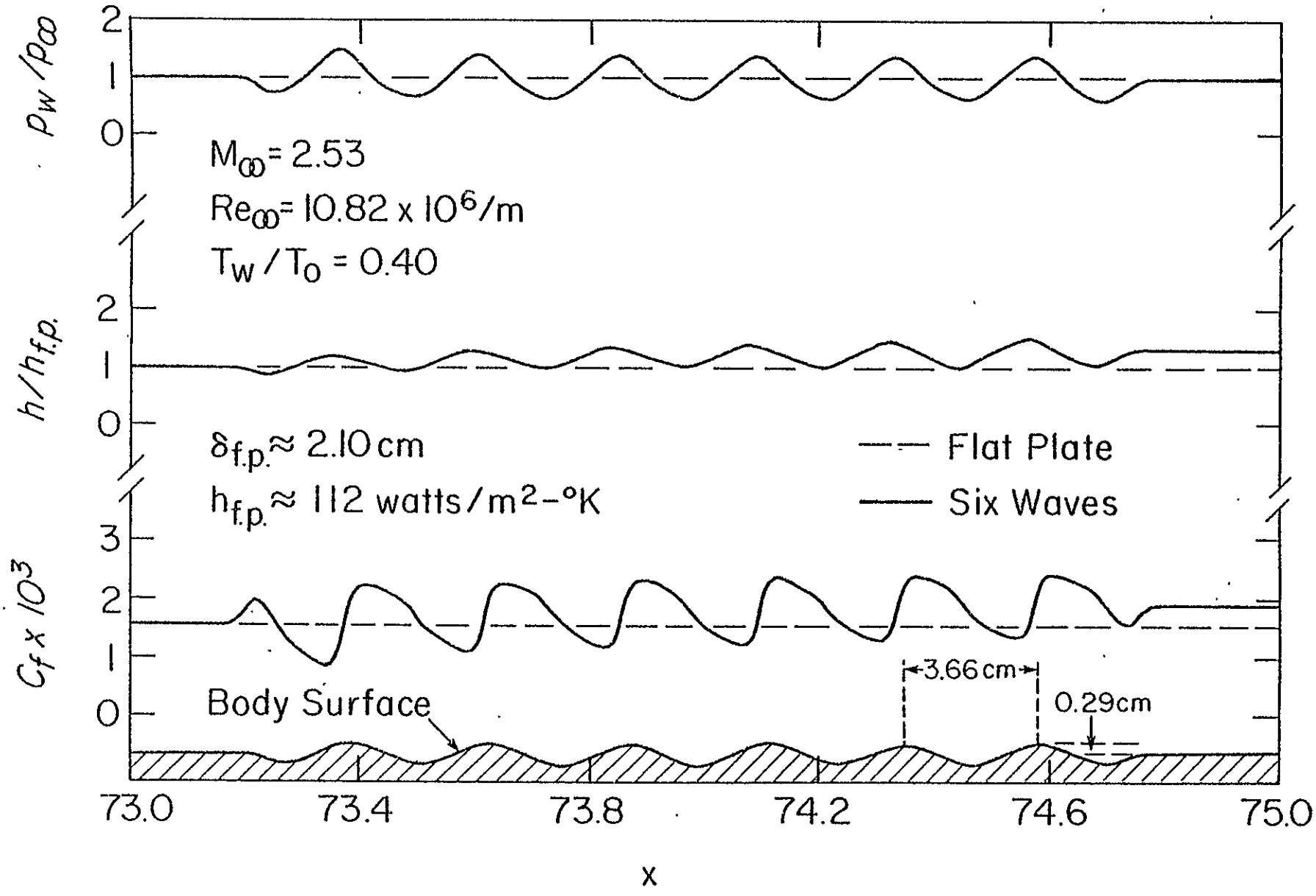

Figure 8A WALL TEMPERATURE EFFECT ON SURFACE PROPERTIE

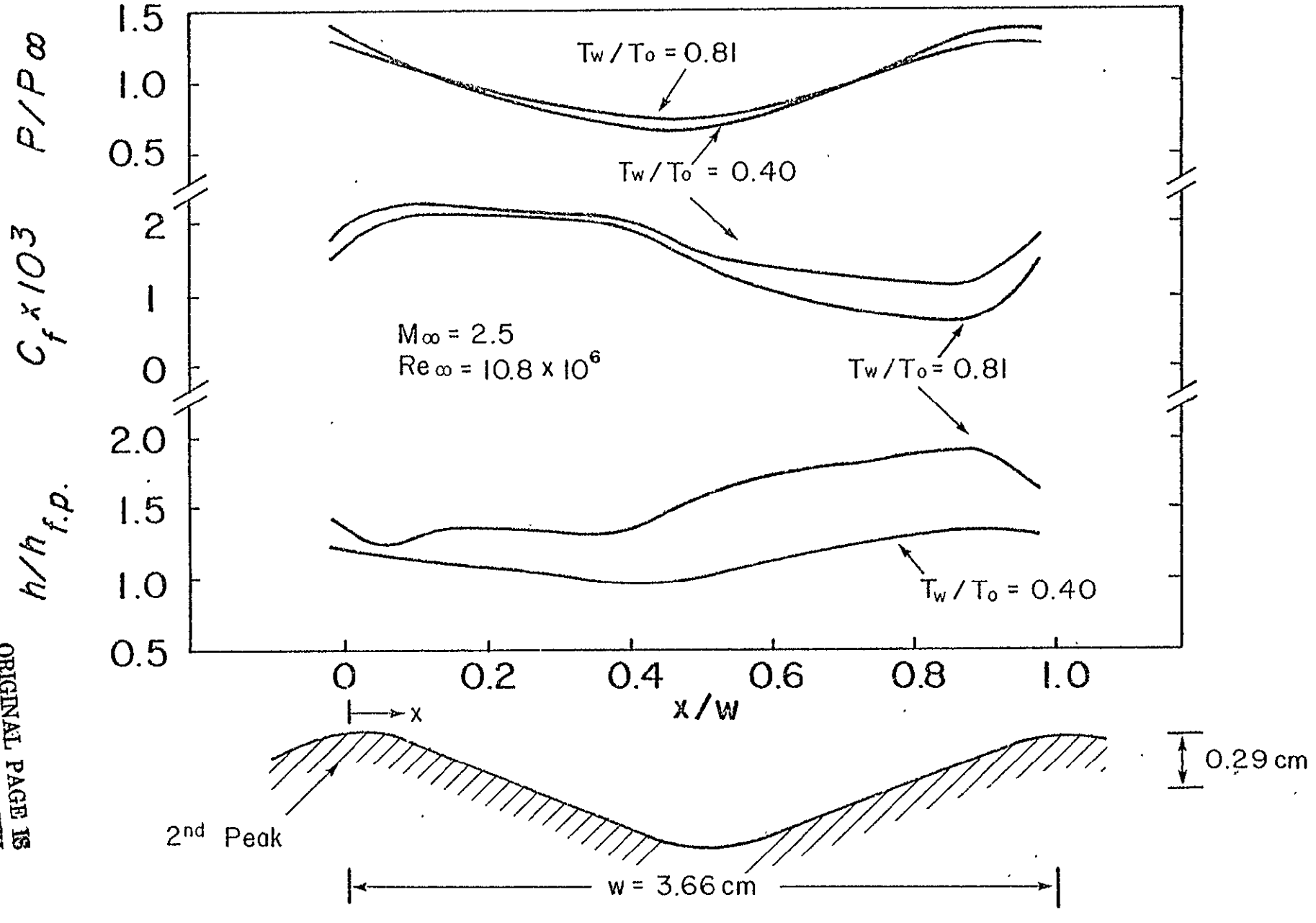

Figure 8B WALL TEMPERATURE EFFECT ON SURFACE PROPERTIES

ORIGINAL PAGE IS
OF POOR QUALITY

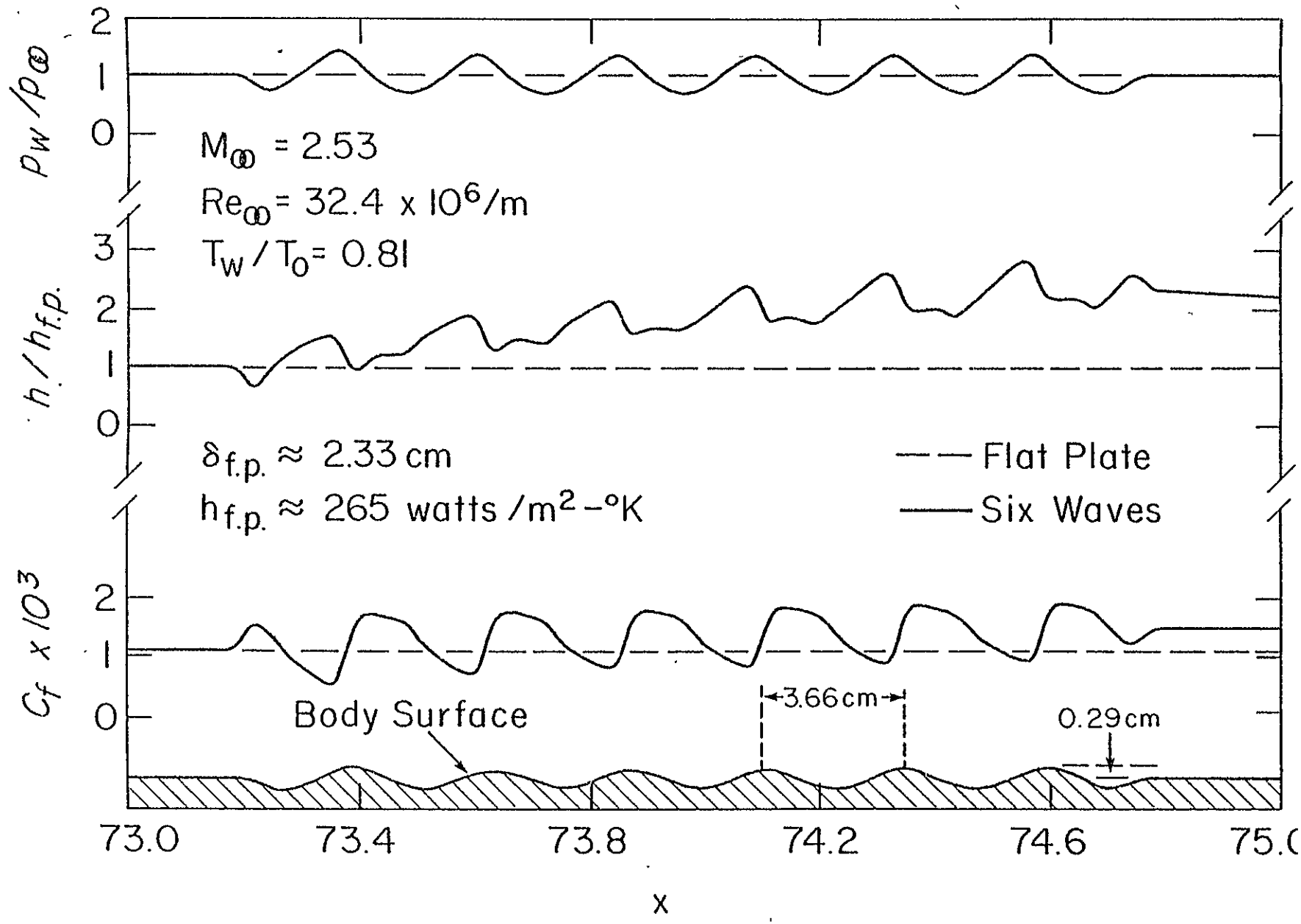
p_w/p_∞
2
1
0
$M_\infty = 2.53$
$Re_\infty = 32.4 \times 10^6/m$
$T_w/T_0 = 0.81$
$h/h_{f.p.}$
3
2
1
0
$\delta_{f.p.} \approx 2.33\,cm$
$h_{f.p.} \approx 265$ watts $/m^2-°K$
Flat Plate
Six Waves
$C_f \times 10^3$
2
1
0
Body Surface
3.66cm
0.29cm
73.0
73.4
73.8
74.2
74.6
75.0
X

ORIGINAL PAGE IS
OF POOR QUALITY

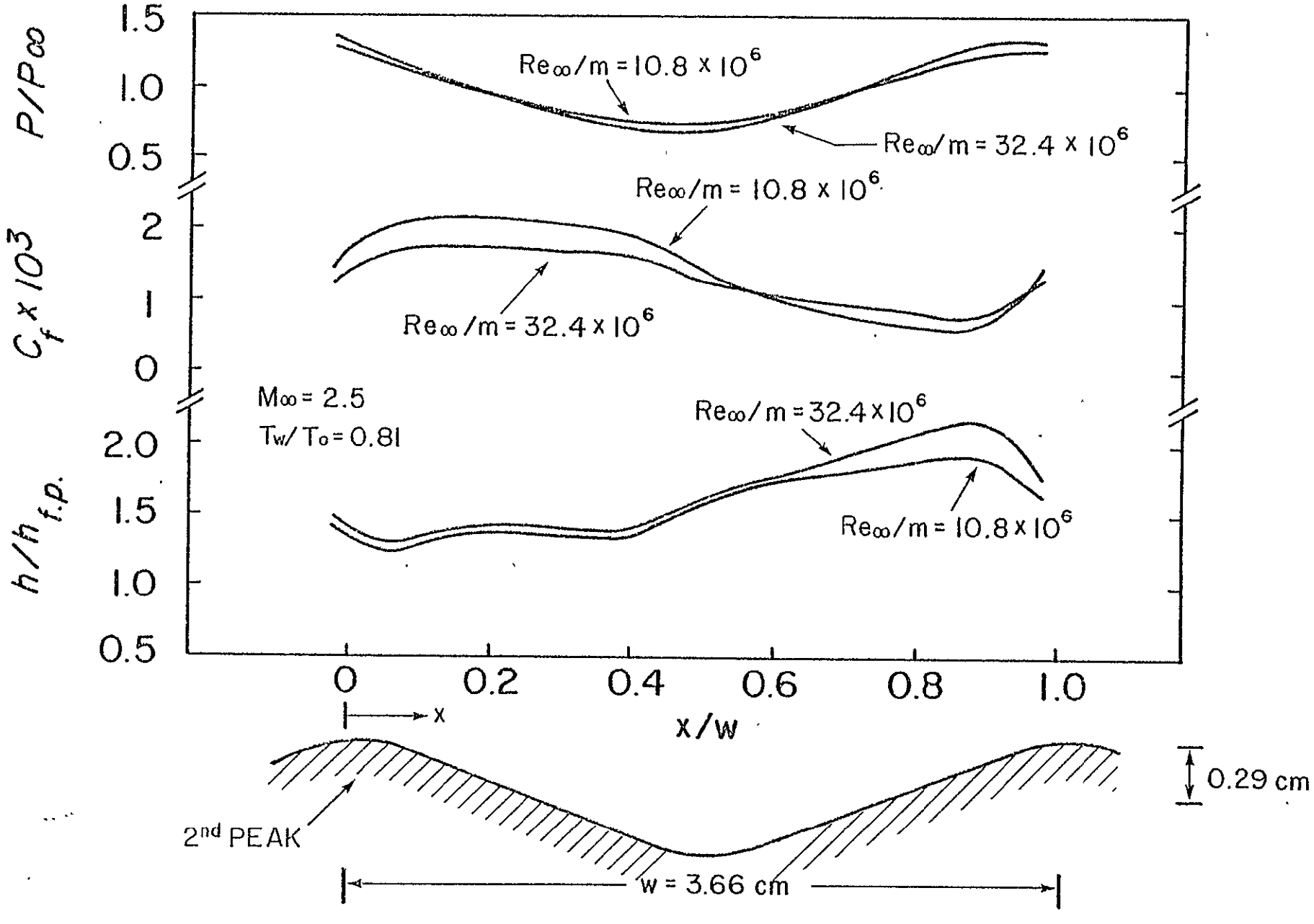

Figure 9B REYNOLDS NUMBER EFFECT ON SURFACE PROPERTIES

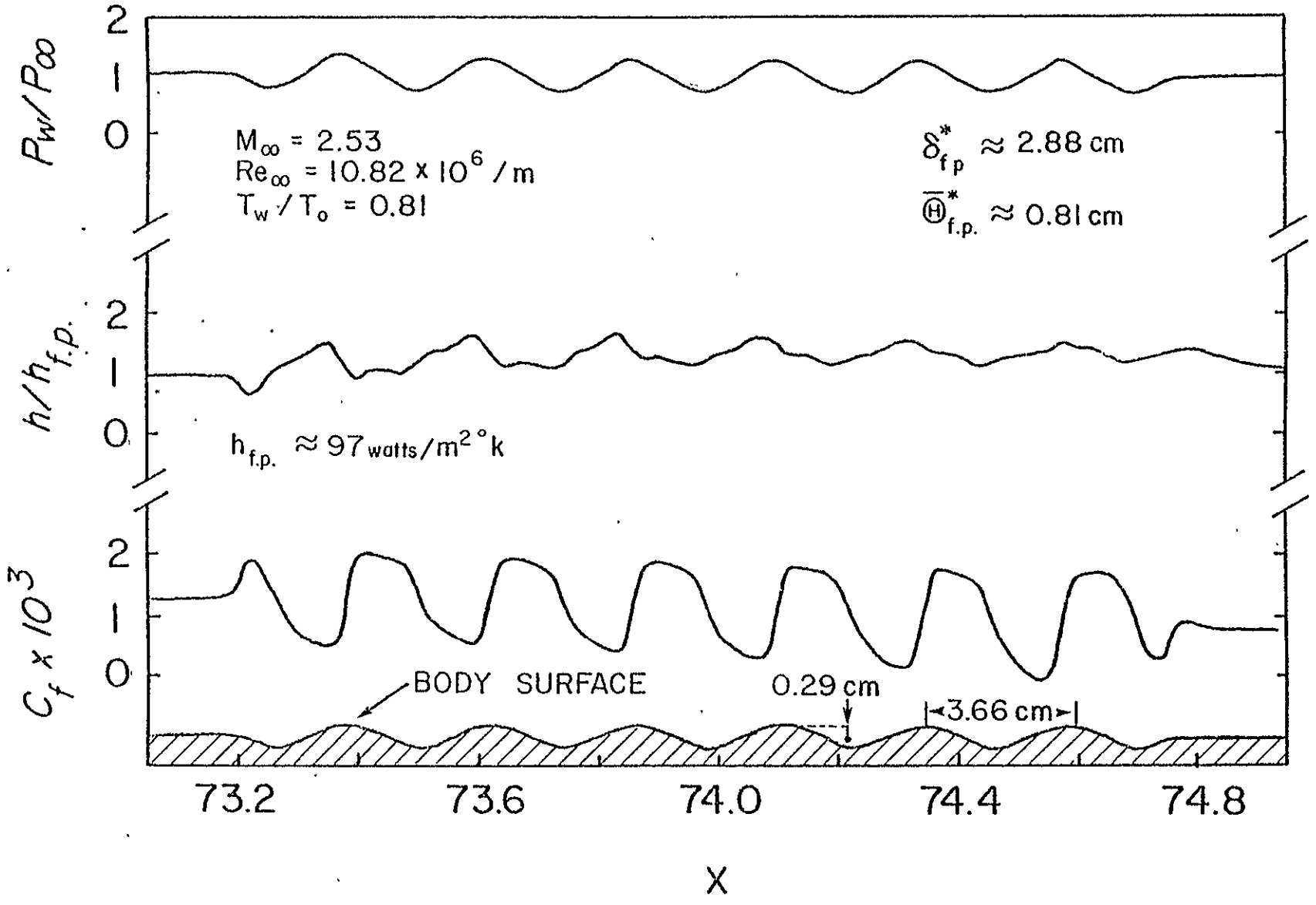

Figure 10A CURVATURE CORRECTION EFFECT ON SURFACE PROPERTIE

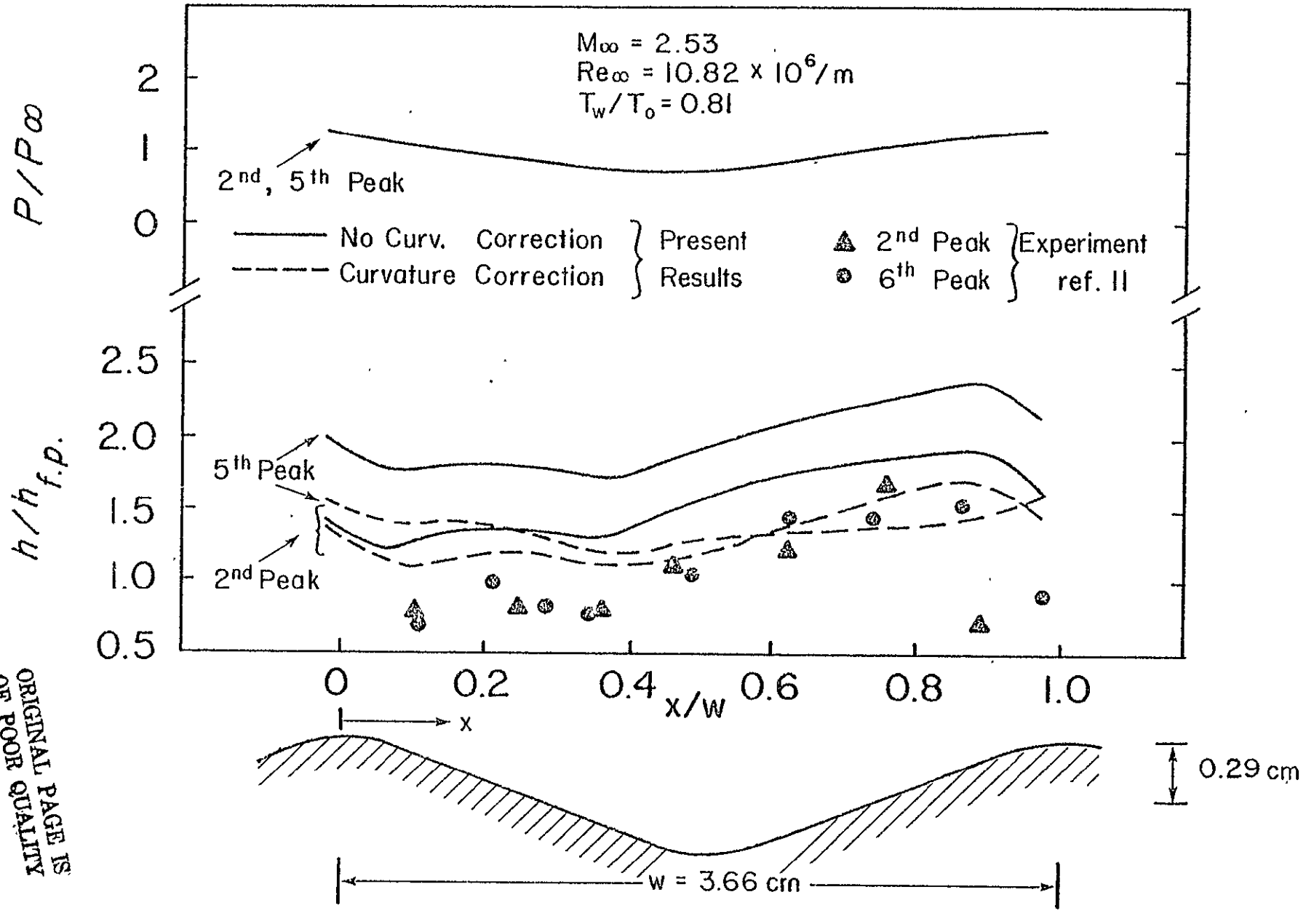

ORIGINAL PAGE IS
OF POOR QUALITY

Figure 10 B CURVATURE CORRECTION EFFECT ON SURFACE PROPERTIES

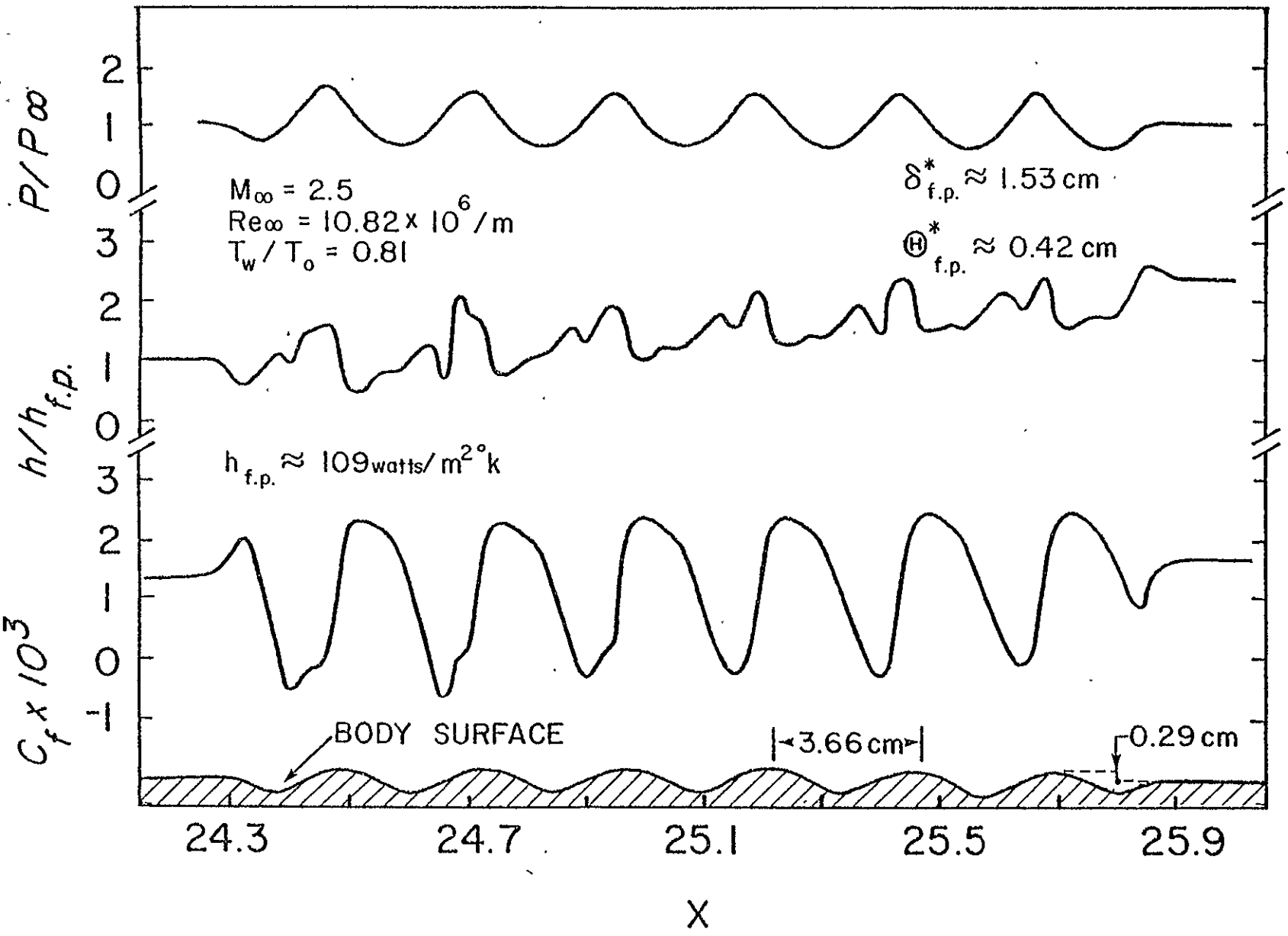

Figure 11A SURFACE PROPERTIES – SEPARATED THICK BOUNDARY LAYE

ORIGINAL PAGE IS
OF POOR QUALITY

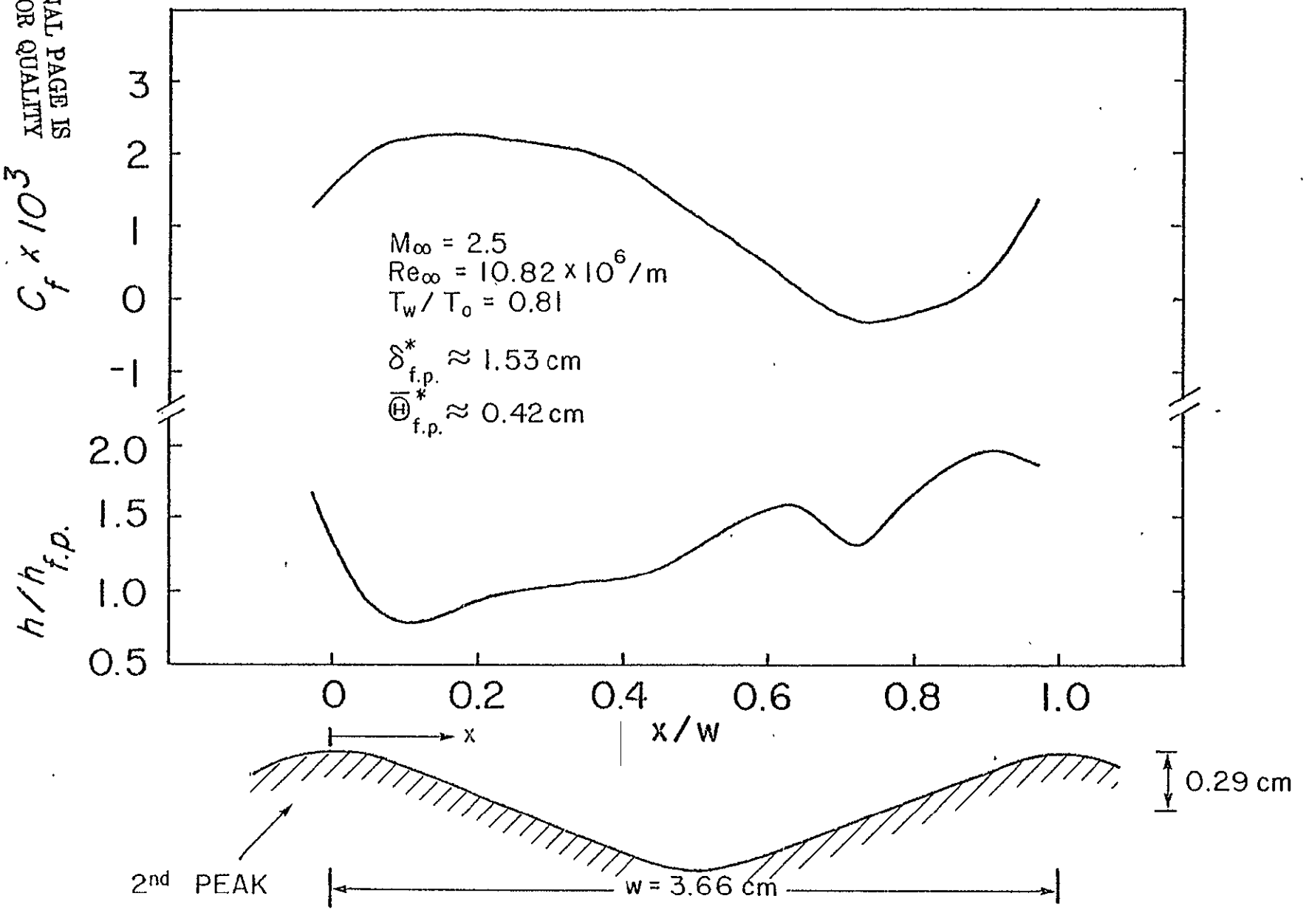

Figure 11B SURFACE PROPERTIES - SEPARATED THICK BOUNDARY LAYE

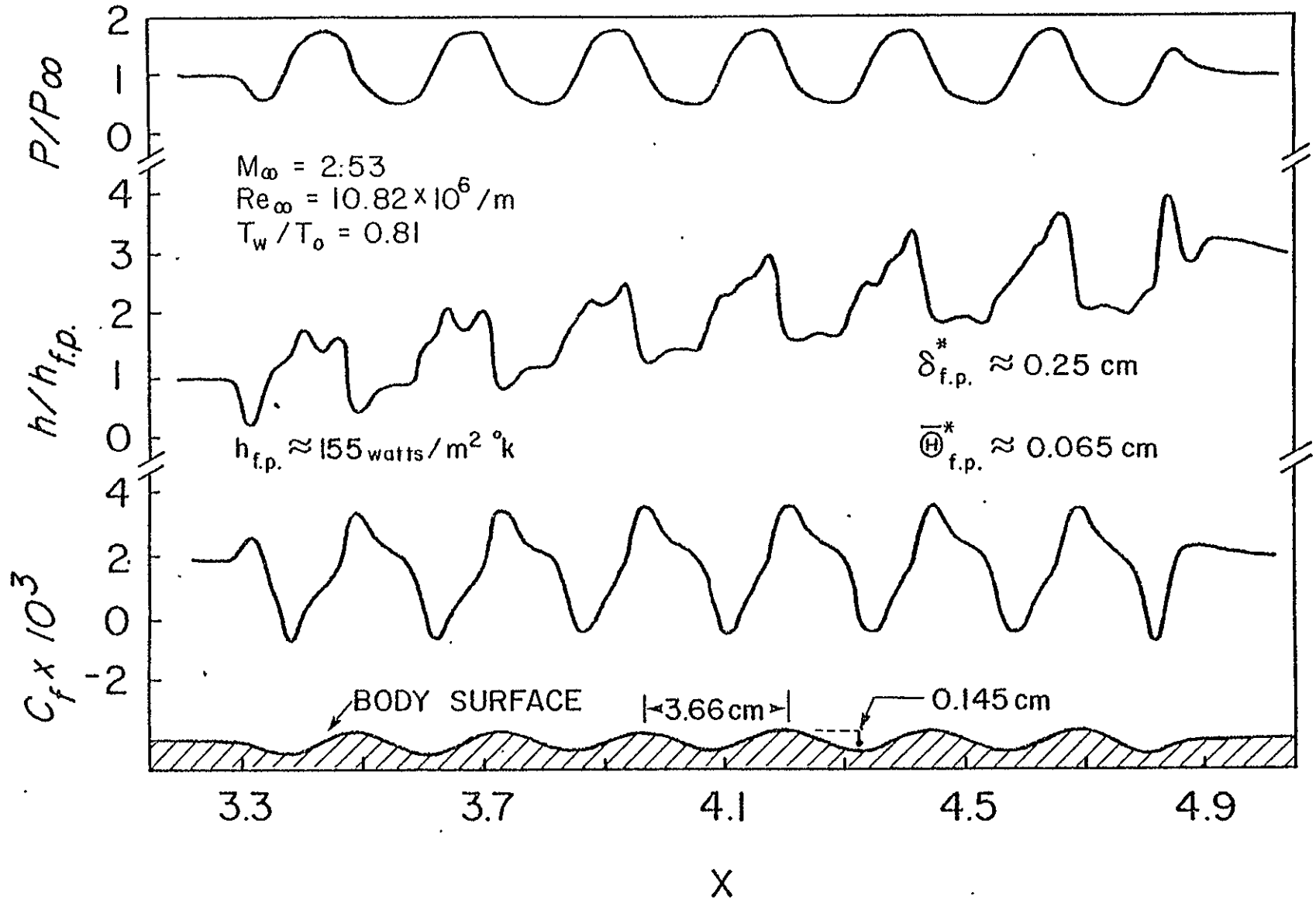

Figure 12 SURFACE PROPERTIES – SEPARATED THIN BOUNDARY LAYEF

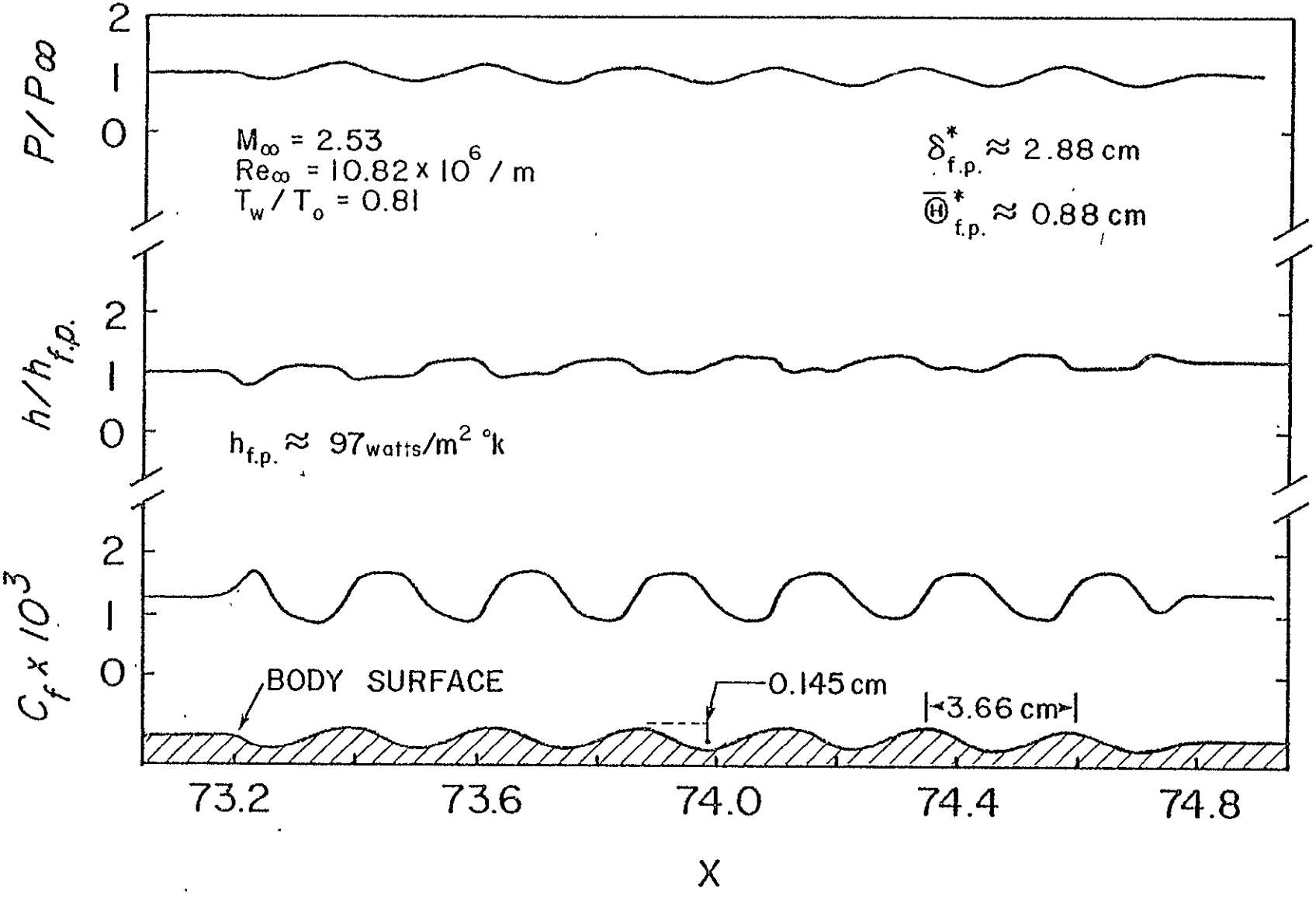

Figure 13A EFFECT OF WAVE HEIGHT ON SURFACE PROPERTIES

ORIGINAL PAGE IS
OF POOR QUALITY

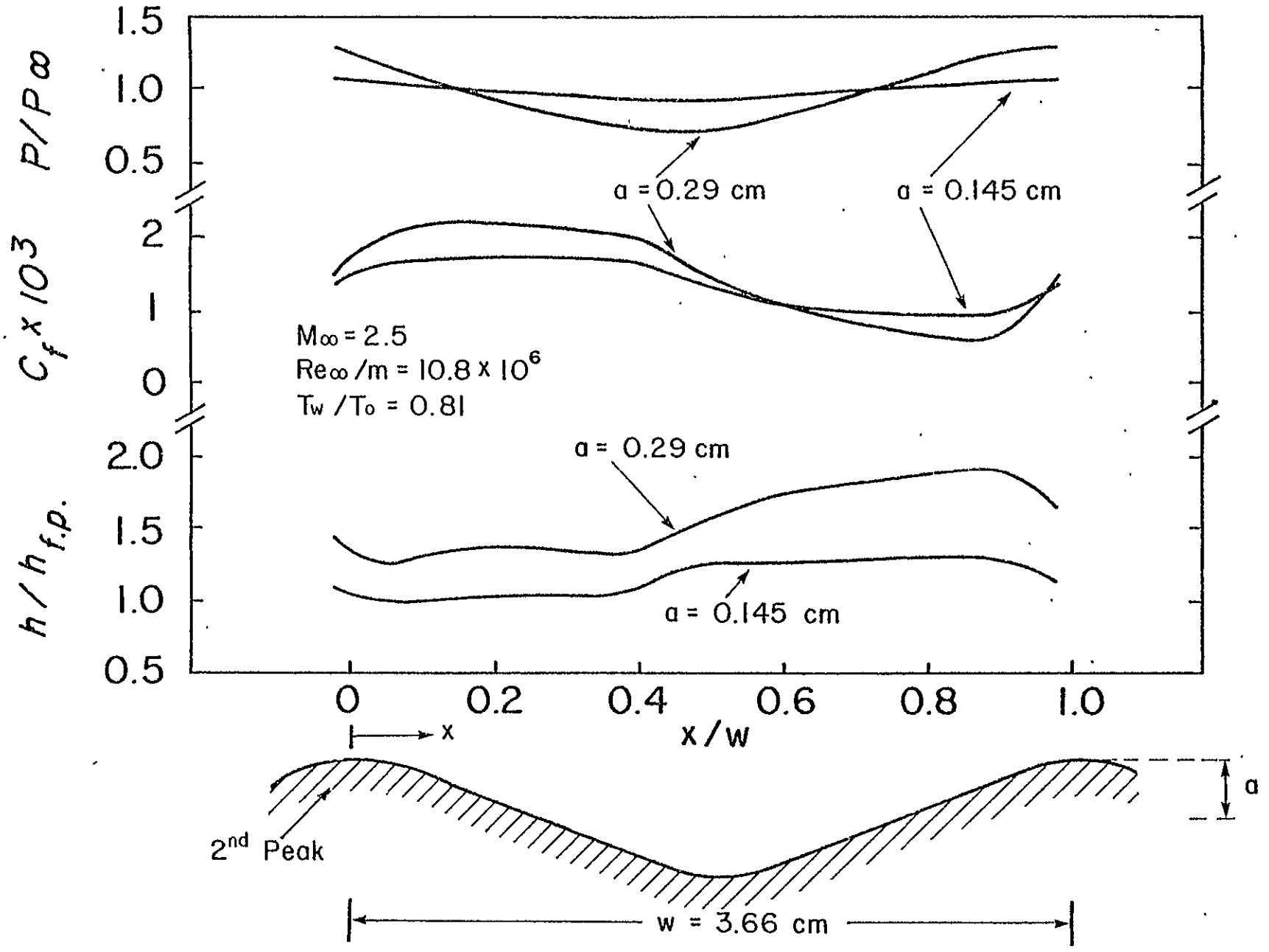

Figure 13 B EFFECT OF WAVE HEIGHT ON SURFACE PROPERTIES

ORIGINAL PAGE IS
OF POOR QUALITY

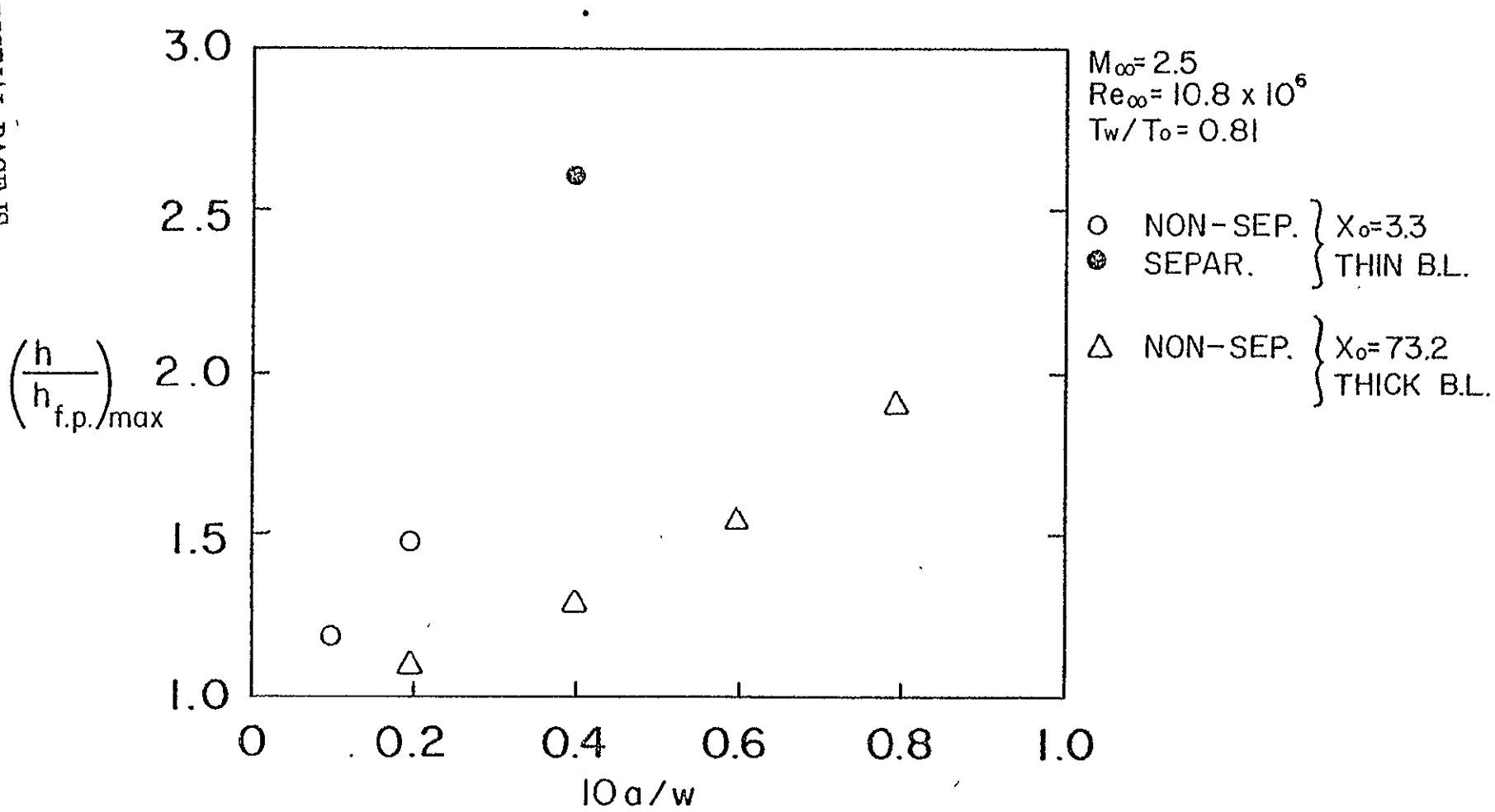

Figure 14 MAXIMUM SURFACE HEATING AT THIRD PEAK